
Fine-grained Out-of-Distribution Detection with Mixup Outlier Exposure

Jingyang Zhang*, Nathan Inkawich*, Yiran Chen, Hai Li
Duke University
jingyang.zhang@duke.edu

Abstract

Enabling out-of-distribution (OOD) detection for DNNs is critical for their safe and reliable operation in the “open world”. Unfortunately, current works in both methodology and evaluation focus on rather contrived detection problems, and only consider a coarse level of *granularity* w.r.t.: 1) the in-distribution (ID) classes, and 2) the OOD data’s “closeness” to the ID data. We posit that such settings may be poor approximations of many real-world tasks that are naturally fine-grained (e.g., bird species classification), and thus the reported detection abilities may be over-estimates. Differently, in this work we make granularity a top priority and focus on *fine-grained OOD detection*. We start by carefully constructing five novel fine-grained test environments in which existing methods are shown to have difficulties. We then propose a new DNN training algorithm, *Mixup Outlier Exposure* (MixupOE), which leverages an outlier distribution and principles from vicinal risk minimization. Finally, we perform extensive experiments and analyses in our custom test environments and demonstrate that MixupOE can consistently improve fine-grained detection performance, establishing a strong baseline in these more realistic and challenging OOD detection settings.

1 Introduction

Out-of-distribution (OOD) detection is the problem of identifying novel data samples during inference time that do not belong to one of the DNN’s known classes. Such detection is crucial for building safe and reliable intelligent systems that operate in the open world. However, OOD detection for DNNs has proven to be difficult, as deep networks are known to have poor confidence calibration [1] and are often implicitly trained under closed-world assumptions [2]. In recent years, many OOD detection algorithms have been proposed, including ones that design post-training scoring mechanisms [3, 4, 5, 6, 7], and others that incorporate specialized training dynamics and regularization terms [8, 9, 10, 11, 12]. In experimentation, these current methods have then shown to be proficient at detecting rather “obviously OOD” inputs (e.g., detecting when an image of a numerical digit is input into a classifier that is only aware of animals and vehicles).

Despite this progress, a key weakness in the design and evaluation of current OOD detection methods is the limited scope of *granularity* that is considered. Here, we define granularity as an intuitive measure of the semantic subtlety/nuance between different categories. For example, a low/coarse granularity task may be to distinguish dogs from birds and cars, whereas a high/fine granularity task may be to distinguish between dog breeds (as shown in Figure 1). As it relates to OOD detection, we specifically refer to granularity across two axis: 1) w.r.t the ID classes; and 2) w.r.t. the OOD data’s “closeness” to the nearest ID class. We posit that current works only cover a coarse level of granularity along either axis. As evidence, consider that perhaps the most common experiment featured in such works is to use the coarse-grained CIFAR-10/100 as the ID task, and the semantically

*Equal contribution.

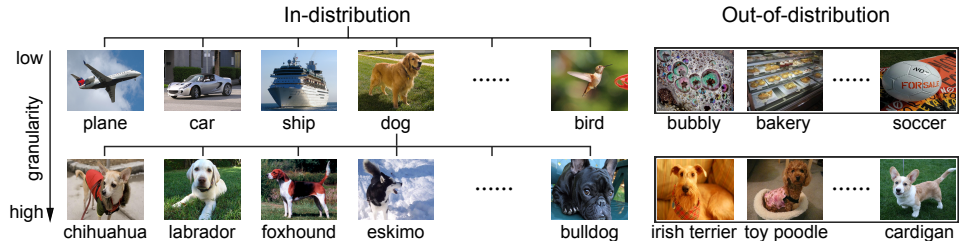


Figure 1: An intuitive example for fine-grained OOD detection.

unrelated SVHN and LSUN datasets as the OOD tasks [4, 6, 7, 5, 9, 13, 14]. While being simple and convenient to setup, we postulate that this experiment represents a rather contrived detection problem that does not closely approximate many real-world tasks where high granularity is expected, e.g., medical image classification [15, 16] and remote sensing applications [17, 18, 19].

Our goal in this work is to make granularity a first-order design consideration by focusing on a setting which we refer to as *fine-grained OOD detection*, which naturally assumes high granularity along both of the aforementioned axis. Specifically, the ID classes cover highly related concepts and the OOD examples can be extremely “close” to the ID data. Figure 1 presents an intuitive example. The first row represents the commonly adopted coarse-grained setting, where the ID classes cover general concepts like plane, car, and bird, while dissimilar concepts such as bubbly texture and soccer ball are used as OOD. The second row represents the fine-grained setting, where the ID task is to recognize a variety of dog breeds, and the OOD task is to identify novel dog breeds. Intuitively, we believe that OOD detection in the fine-grained setting is more challenging yet realistic, and therefore it becomes the focus of this work.

Ultimately, we make two key technical contributions to OOD detection research. First, we build five novel test environments for fine-grained OOD detection in the domain of natural imagery. We leverage publicly available fine-grained classification datasets and create ID/OOD splits using an original ranking-based holdout class method. Second, we further propose a new DNN training algorithm called *Mixup Outlier Exposure (MixupOE)*, which consistently achieves higher OOD detection rates across our five fine-grained OOD detection benchmarks. Functionally, MixupOE leverages both empirical and vicinal distributions [20, 21] defined using ID and OOD samples at training time. Different from previous works, our methodology explicitly defines the decay of prediction confidence as the input transitions from an ID sample to an OOD sample. In addition to empirical evaluations of OOD detection rates, we also perform several analyses to help explain *why* MixupOE performs well in these fine-grained OOD settings.

2 Related work

OOD Detection Approaches. Many popular works in OOD detection research use a pre-trained DNN classifier as a base model/feature-extractor, and design an OOD scoring mechanism that leverages some signal from this model. Several methods utilize the output space of the classifier. Hendrycks et al. [11] establish maximum softmax probability (MSP) as a baseline method. Liang et al. [4] improves upon MSP with temperature scaling and input pre-processing. Liu et al. [5] develop an energy-based score using the DNN’s logits. Other works focus on the intermediate feature space of DNNs. For example, Lee et al. [6] compute Mahalanobis distance to measure the probability density of inputs, and Sastry and Oore [7] identify abnormal activation patterns with Gram Matrices.

Another line of research modifies the base DNN’s training phase. Lee et al. [10] synthesize OOD samples with a GAN and force the classifier to be less confident on the generated OOD data. Hendrycks et al. [11] design a regularization term that uses a diverse and realistic distribution to also encourage low confidence predictions on OOD data. Recently, several self-supervised learning methods have also been adapted to enhance detection ability [22, 23]. Our work is perhaps most closely related to [11] in that we too use an outlier training set, however, our method uniquely formulates the learning procedure with vicinal distributions. We remark that the above works all consider relatively coarse-grained settings in their experiments.

Finally, worth mentioning are a number of methods that rely on generative models. These methods have the intuitive advantage of being able to directly yield an estimated likelihood of the inputs, i.e.,

$p(x)$ [24, 25, 26, 27]. However, such generative methods are also known to have difficulties scaling to the data dimensionalities used in our new benchmarks (i.e., 512×512 px spatial resolution) [28, 24].

Towards Granular OOD Detection. Perhaps most relevant, there are a small number of recent works that purposefully consider settings where the test OOD samples are semantically related to the ID classes [23, 29, 30, 13]. Recall, this fits within our second axis of granularity discussed in Section 1. The critical difference between our fine-grained OOD setting and these is that we also assume high granularity w.r.t. the ID classes. We argue that this is a crucial distinction because without such ID granularity it may be debatable whether a model *should* be asked to detect granular OOD samples! For example, consider an experiment in Winkens et al. [13] that regards “leopard” (in CIFAR-100) as a granular OOD sample for a CIFAR-10 model (which contains a “cat” class). This situation begs the question: given a model trained on cats, is it more desirable to generalize to the notion of a leopard, or to identify leopards as OOD? We posit that this is an ill-posed question for a general OOD benchmark because either of the decisions may be correct, depending on the application. In our fine-grained OOD settings, we work to avoid such ambiguities through more careful construction of the ID and OOD tasks.

3 Challenges of fine-grained OOD detection

This section serves to further motivate a detailed study on fine-grained OOD detection. In Section 3.1 we describe the construction of the five fine-grained test environments used in this paper, which is necessary because there are no existing benchmarks. In Section 3.2, through initial evaluations we show that fine-grained OOD detection presents distinct challenges for existing methods. Lastly, in Section 3.3 we present a preliminary analysis on *why* current methods have difficulty in the fine-grained OOD setting, which directly inspires our MixupOE methodology.

3.1 Test environments

The test environments are curated from five public fine-grained visual classification (FGVC) datasets, namely Caltech-UCSD Birds [31], ThuDogs [32], Oxford Flowers [33], Stanford Cars [34], and FGVC-Aircraft [35]. We refer to them as *Bird*, *Dog*, *Flower*, *Car*, and *Aircraft*, respectively. For each dataset, we create an ID/OOD split using a holdout class method, i.e., we keep some of the categories as ID and the rest are held out from the training set and considered OOD at test time.

At first thought, a straightforward way to establish the ID/OOD splits would be to simply randomly partition the datasets. However, we find that there is a large variance in both the OOD detection rates and the test accuracy that depends on which exact classes remain in the ID split (or similarly, which classes make up the holdout OOD split). To show this experimentally, we randomly sample 10-class ID splits from the *Bird* dataset and measure the accuracy and OOD detection rates (on the remaining holdout classes) after training. Figure 2 shows the results of this experiment, where the splits are sorted by AUPR (i.e., OOD detection performance). From looking at the ranges on the y-axis, there is clearly a significant dependence of both accuracy and detection rates on the split index, which we believe is an undesirable consequence of random partitioning and may harm the reproducibility of results.

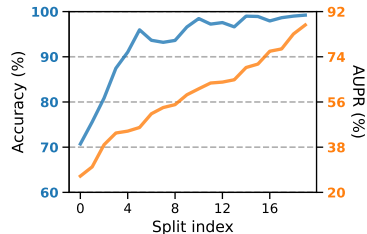


Figure 2: Accuracy and detection AUPR (using MSP) of various 10-class splits taken from the *Bird*.

To build benchmarks for fine-grained OOD detection, we believe it is important to isolate the detection task from other possible influences, e.g., classification accuracy and calibration on ID data [36, 37]. This will allow the benchmarks to more purely reflect the difficulties of the detection task itself. As an example, we posit that focusing on the 0th split in Figure 2 may not be the most informative benchmark test because the impact of poor ID accuracy may be a dominating factor in the poor detection performance. Thus, we propose to use a class-wise ranking mechanism to guide the selection of the ID/OOD splits. Starting with a pre-trained classifier on all classes of the dataset, we assign a score to each class which factors in both accuracy and the average entropy of predictions on test samples from that class. The ID split is then constructed using the classes on which the model is most accurate and confident, while the remaining classes make up the holdout OOD split. In practice, using this proposed ranking mechanism we construct one ID/OOD split for each of the five FGVC

Table 1: Detection performance (in % AUPR) of existing methods in fine-grained OOD settings. * implies the implementation does not exactly follow the original design.

Method	Bird		Dog		Flower		Car		Aircraft	
	Places365	holdout								
MSP [3]	94.3±1.0	67.6 ±0.3	97.6±0.4	48.6 ±0.9	98.5±0.1	83.6±2.5	94.5±0.7	75.3 ±0.5	92.8±1.5	42.7 ±2.1
ODIN* [4]	96.7±0.4	60.4±0.6	99.4±0.1	46.4±0.5	99.2±0.1	82.4±1.9	98.0±0.3	71.4±1.0	95.4±1.0	39.6±2.1
Energy [5]	96.8±0.6	54.6±0.7	99.5±0.1	44.5±0.5	99.1±0.1	78.3±1.8	98.4±0.2	67.3±1.2	95.7±0.9	38.0±2.2
Mahalanobis* [6]	91.0±0.5	24.0±0.3	31.1±1.1	23.6±0.2	97.6±0.3	43.5±1.0	78.3±0.3	25.0±0.2	98.4±0.2	14.5±0.1
Gram Matrices* [7]	88.6±1.9	50.7±1.1	91.2±1.3	35.2±0.3	94.8±0.7	69.2±2.4	93.6±1.5	54.9±0.5	96.1±0.9	27.6±1.0
Rotation [22]	82.0±4.0	42.9±1.5	92.0±4.3	42.1±1.5	48.4±1.2	32.5±2.1	99.7±0.1	67.8±0.1	97.3±0.6	36.1±2.8
OE [11]	99.2 ±0.2	67.3±1.3	98.4±0.7	48.6±1.3	99.7 ±0.1	85.1 ±1.7	99.0±0.2	72.6±0.9	99.5±0.1	40.7±1.0
EnergyOE [5]	98.3±0.3	51.8±0.7	99.7 ±0.0	45.7±1.7	99.7±0.1	84.8±1.6	99.3 ±0.2	67.4±1.3	99.6 ±0.1	36.9±2.3

datasets. Importantly, we let each ID split consist of about 100 classes so that the formed detection problems are sufficiently challenging and may approximate real-world complexity. See Appendix A for more details on the ranking methodology and Appendix B for details of the dataset splits.

3.2 Evaluating existing methods

With these benchmarks, our first objective is to evaluate existing OOD detection methods to assess their performance in fine-grained OOD settings. We consider eight state-of-the-art detectors, including five post-training scorers [3, 4, 5, 6, 7] and three that incorporate training-time regularizations [22, 11, 5]. In each test, in addition to detecting the holdout samples, we also consider distinguishing samples from the Places365 [38] dataset to represent a coarse detection task. Finally, to measure detector performance, we use three common metrics [4]: false positive rate at a 95% true positive rate (FPR95); area under the receiver operating characteristic curve (AUROC); and area under the precision-recall curve (AUPR). See Appendix C for more details regarding experimental setup and Appendix D for implementation details of the detection methods.

Table 1 shows the AUPR detection results for this experiment, while the expanded table is in Appendix E. Our main observation is that in 4 out of 5 benchmarks, on the holdout OOD data no method performs better than MSP, which simply thresholds the softmax prediction confidence! Interestingly, this finding contrasts detection results on the Places365 data, where more advanced methods consistently outperform MSP [4, 5, 6, 7, 22, 11]. We believe that these trends clearly demonstrate that the progress made in the coarse-grained OOD detection setting does not implicitly translate to the fine-grained one, further motivating our work.

3.3 Preliminary analysis

Our next objective is to analyze *why* fine-grained OOD detection is particularly difficult? For this analysis we use the MSP [3] and OE [11] detection methods, which are among the most effective as shown in Table 1. They are also representative of two primary detection methodologies: MSP is a post-training scoring mechanism that is applied to a DNN trained in a “standard” way (i.e., by minimizing an average cross-entropy loss over an ID-only training dataset); and OE modifies the DNN’s training procedure to explicitly regularize the model’s outputs against OOD samples, so after training a threshold can be applied to the prediction confidence (same concept as MSP in the post-training stage). Since both methods functionally threshold the DNN’s confidence at test time, our concept for analysis is to forward pass different data samples through the underlying Standard- and OE-trained models and monitor the distributions of prediction confidence scores. This type of analysis allows us to more clearly see how the models are interpreting the ID/OOD data, beyond the high level detection statistics described in Section 3.2.

One way we leverage this analysis concept is to directly forward pass the ID/OOD samples from the *Dog* benchmark through the Standard and OE models and visualize the prediction confidence distributions with density plots, as shown in Figure 3 (see Appendix F for results on the other datasets). Our main takeaway here is that while OE indeed helps the model yield lower confidence predictions when facing Places365 data, it does not have the same effect on the holdout data. Rather, the holdout confidence distribution for the OE model is very similar to the Standard model’s holdout distribution. Based on the intuition that holdout samples are much “closer” to ID samples due to their strong semantic similarity [12], our hypothesis for the observation in Figure 3 is that current models (even trained with OE) are not well calibrated in the “near-ID” region. This hypothesis directly motivates the further study in our next analysis.

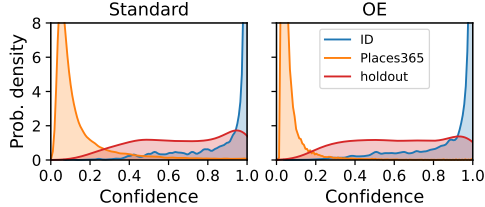


Figure 3: Confidence density plot of ID and OOD samples.

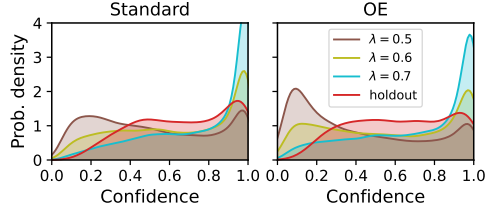


Figure 4: Confidence density plot of interpolated samples.

To study the proposed hypothesis more carefully, our second analysis uses the same methodology but focuses more intently on the behavior of the models in the “near-ID” regions, and goes beyond the holdout measurements in Figure 3. For this analysis, we craft another type of near-ID sample (other than the holdout data) by linearly interpolating between ID and “far-away” OOD samples (from Places365 in our case) in the pixel space, i.e., $x_{\text{test}} = \lambda x_{\text{ID}} + (1 - \lambda)x_{\text{OOD}}$. We then forward pass many of these interpolated test samples at $\lambda = \{0.5, 0.6, 0.7\}$ through both of the models and again monitor their prediction confidence distributions. Figure 4 shows the results of this experiment for the *Dog* splits and Appendix F shows results for the other benchmarks. The major observation from this experiment is that both models are indeed not well calibrated in the near-ID region as characterized by the interpolated inputs. Using $\lambda = 0.7$ as a key example, ideally one would expect that the prediction confidences from a well-calibrated model would not have so much density in the ~ 1.0 confidence region, because the inputs only contain 70% “relevant” information from the ID samples. So, the over-confidence exhibited by the models, especially at $\lambda = 0.6, 0.7$, is another indicator of why these models have difficulty detecting fine-grained OOD data. Overall, we believe that this series of analysis has exposed the problem of current models being poorly calibrated in the near-ID region, which motivates our MixupOE approach described in the next section.

4 Mixup Outlier Exposure

To improve OOD detection in the fine-grained setting, we propose to explicitly regularize the model’s behaviour in the near-ID region. Our key methodological insight is to control how the DNN’s prediction confidence decays as the input image transitions between ID and OOD samples. To gain the necessary intuition for our method, first consider the training objective of vanilla Outlier Exposure (OE) [11], which is formulated as

$$\mathbb{E}_{(x,y) \sim \mathcal{D}_{\text{in}}, x' \sim \mathcal{D}_{\text{out}}^{\text{OE}}} [\mathcal{L}(f(x), y) + \beta \mathcal{L}(f(x'), \mathcal{U})]. \quad (1)$$

Here, \mathcal{D}_{in} is the ID training dataset where (x, y) is a labeled sample, $\mathcal{D}_{\text{out}}^{\text{OE}}$ is the OOD training distribution that contains a large and diverse set of outlier samples x' , $\mathcal{L}(f(x), y)$ is the cross-entropy loss between the DNN’s predicted distribution $f(x)$ and the ground truth distribution y , \mathcal{U} is the uniform distribution over the ID classes, and β is a weighting term. The OE objective can be interpreted as an *empirical risk minimization* (ERM) over samples in both \mathcal{D}_{in} and $\mathcal{D}_{\text{out}}^{\text{OE}}$, where predictions on ID samples should be maximally confident (i.e., resemble a one-hot distribution), while outputs on OOD training samples should have maximum entropy/uncertainty (i.e., resemble a uniform distribution). The test-time OOD score is then taken as the maximum prediction confidence level. Critically, notice that OE has no control over the in-between region of ID and OOD, especially in the *vicinity* [20] of the ID region in where fine-grained OOD images are likely to locate [12].

To improve upon the concept of OE by tailoring it for the fine-grained setting, we propose *Mixup Outlier Exposure* (MixupOE), which leverages a vicinal distribution w.r.t. the empirical samples in \mathcal{D}_{in} and $\mathcal{D}_{\text{out}}^{\text{OE}}$. We do this by training our DNNs within a hybridized ERM and *Vicinal Risk Minimization* (VRM) [20] framework. For the ERM components, we can directly use the samples in \mathcal{D}_{in} and $\mathcal{D}_{\text{out}}^{\text{OE}}$ in a way very similar to OE. For the VRM components, we leverage vicinal distributions by training on “virtual” samples constructed with the Mixup algorithm [21]. Specifically, Mixup creates virtual training samples (\tilde{x}, \tilde{y}) by linearly interpolating between two empirically observed samples (x_1, y_1) and (x_2, y_2) in both the data space and the label space, i.e., $\text{mixup}((x_1, y_1), (x_2, y_2), \lambda) = (\tilde{x}, \tilde{y}) = (\lambda x_1 + (1 - \lambda)x_2, \lambda y_1 + (1 - \lambda)y_2)$, where $\lambda \sim \text{Beta}(\alpha, \alpha)$ for an introduced hyperparameter α .

Importantly, within MixupOE’s hybrid ERM-VRM framework there is opportunity for training on four separate terms (distributions): “ID” (\mathcal{D}_{in}), “ID-ID” ($\mathcal{D}_{\text{in-in}}$), “ID-OOD” ($\mathcal{D}_{\text{in-out}}$), and “OOD” ($\mathcal{D}_{\text{out}}^{\text{OE}}$).

Training on “ID” means we are minimizing empirical risk on samples directly from \mathcal{D}_{in} . Training on “ID-ID” means we are minimizing vicinal risk on virtual samples from $\mathcal{D}_{\text{in-in}}$, which are constructed using two samples drawn from \mathcal{D}_{in} (i.e., $\text{mixup}((x_1, y_1) \sim \mathcal{D}_{\text{in}}, (x_2, y_2) \sim \mathcal{D}_{\text{in}})$). Training on “ID-OOO” means we are minimizing vicinal risk on virtual samples from $\mathcal{D}_{\text{in-out}}$, which are constructed using one sample from \mathcal{D}_{in} and another from $\mathcal{D}_{\text{out}}^{\text{OE}}$ (i.e., $\text{mixup}((x_1, y_1) \sim \mathcal{D}_{\text{in}}, (x_2 \sim \mathcal{D}_{\text{out}}^{\text{OE}}, \mathcal{U}))$). And, training on “OOO” means we are minimizing empirical risk on samples directly from $\mathcal{D}_{\text{out}}^{\text{OE}}$. Overall, the full MixupOE training objective with all four terms can be written as:

$$\mathbb{E}_{(x,y) \sim \mathcal{D}_{\text{in}}} [\mathcal{L}(f(x), y)] + \beta_{\text{in-in}} \mathbb{E}_{(\tilde{x}, \tilde{y}) \sim \mathcal{D}_{\text{in-in}}} [\mathcal{L}(f(\tilde{x}), \tilde{y})] + \beta_{\text{in-out}} \mathbb{E}_{(\tilde{x}', \tilde{y}') \sim \mathcal{D}_{\text{in-out}}} [\mathcal{L}(f(\tilde{x}'), \tilde{y}')] + \beta_{\text{out}} \mathbb{E}_{(x') \sim \mathcal{D}_{\text{out}}^{\text{OE}}} [\mathcal{L}(f(x'), \mathcal{U})], \quad (2)$$

where $\beta_{\text{in-in}}$, $\beta_{\text{in-out}}$, β_{out} are hyperparameters for weighting the terms. Also, although omitted in equation (2), it is implied that we have two additional hyperparameters $\alpha_{\text{in-in}}$ and $\alpha_{\text{in-out}}$ for the corresponding Mixup operations.

Intuitively, we believe that the “ID-ID” and “ID-OOO” terms have the potential to help improve OOD detection for several reasons. From one perspective, training on virtual samples from random pairs of ID and OOD data at random λ values effectively increases the training dataset size in a meaningful way. This may provide the DNN with a better characterization of a broader area of the input space, and specifically in the near-ID regions. Also, the corresponding interpolated soft targets will provide strong regularization over the covered region by encouraging the model to calibrate its prediction confidence on those mixed samples. Specifically, the “ID-ID” term may mainly affect the near-ID region since the virtual samples are crafted using only ID data, while the “ID-OOO” is able to cover a broader area of the input space and may have implications in both fine and coarse OOD detection.

Initial Ablation Study. Before moving on, we acknowledge that although MixupOE exposes the opportunity to leverage four terms, it is unclear whether all of them are necessary. As an initial ablation study, we investigate how different combinations of the four terms in equation (2) will affect the trained model’s OOD detection performance. Using a similar experimental setup to the one described in Section 3.2, Table 2 shows the OOD detection performance (measured with AUPR) as we use different compositions of the terms. Note, we use the *Bird* splits as the fine-grained OOD task to collect these results.

Interestingly, we find that including all of the terms into the optimization does *not* necessarily lead to the best performance. There appears to be conflicts between some objectives which are most apparent in the fluctuating performance on the holdout set. We suspect this behavior is the result of manifold intrusion [39], a subtle under-fitting problem in the Mixup framework that results from assigning distinct synthetic labels to visually similar interpolated samples. In an effort to balance simplicity and effectiveness, we identify that using only the “ID” and “ID-OOO” components leads to high performance on both the coarse OOD Places365 data and the fine OOD hold-out data. For this reason, throughout the remainder of this work we simplify MixupOE as:

$$\mathbb{E}_{(x,y) \sim \mathcal{D}_{\text{in}}} [\mathcal{L}(f(x), y)] + \beta_{\text{in-out}} \mathbb{E}_{(\tilde{x}, \tilde{y}) \sim \mathcal{D}_{\text{in-out}}} [\mathcal{L}(f(\tilde{x}), \tilde{y})]. \quad (3)$$

We leave it as a future work to perform further investigations into whether or not this two term simplification of the full MixupOE is adequate in all settings.

Hyperparameter Tuning. Our simplified MixupOE algorithm now has two hyperparameters: $\alpha_{\text{in-out}}$ parameterizes the Beta distribution for the `mixup` operation that constructs $\mathcal{D}_{\text{in-out}}$; and $\beta_{\text{in-out}}$ weights the contribution of the “ID-OOO” term in equation (3). Following [11, 5], we choose the hyperparameter values such that the OOD detection performance is maximized on a group of validation outliers $\mathcal{D}_{\text{out}}^{\text{val}}$, while the ID classification accuracy is minimally affected. Importantly, $\mathcal{D}_{\text{out}}^{\text{val}}$ is fully synthetic and reveals no information about the test-time OOD distribution $\mathcal{D}_{\text{out}}^{\text{test}}$. In Appendix D.3, we give the hyperparameter values used in this work and also perform experiments to show that MixupOE is not extremely sensitive to either of these hyperparameters.

Table 2: AUPR results using different compositions of MixupOE objectives

objectives				Places365	holdout
ID	ID-ID	ID-OOO	OOD		
✓				94.3±1.4	67.8±0.3
✓			✓	99.2±0.2	67.3±1.3
✓	✓			92.5±2.0	69.7±0.7
✓		✓		97.5±0.7	70.0±0.9
✓	✓	✓		96.3±0.8	70.3±1.4
✓	✓		✓	83.4±2.0	53.1±0.4
✓		✓	✓	98.0±0.4	62.4±1.8
✓	✓	✓	✓	96.0±2.3	61.7±3.9

5 Experiments

5.1 Setup

Training. Regardless of the specific detection method, we start by training ResNet-50s [40] on each of the ID datasets using a vanilla cross-entropy loss (referred to as the “Standard” models). For the OE/EnergyOE/MixupOE methods we then do an additional 10 epochs of fine-tuning with the respective objectives (as done in [11, 5]). The outlier training set \mathcal{D}_{out}^{OE} we consider for these methods is WebVision 1.0 [41], which contains millions of natural images crawled from Flickr and Google. We believe this dataset represents a realistic construction of \mathcal{D}_{out}^{OE} . Importantly, to avoid arguments of “cheating” we filter out relevant images to the holdout OOD task from \mathcal{D}_{out}^{OE} (e.g., all dog images are removed from \mathcal{D}_{out}^{OE} during the *Dog* test). Additional details are discussed in Appendix D.

Evaluation. The evaluation procedure follows the one described in Section 3.2 (also see Appendix C and D). We consider eight state-of-the-art methods as baselines [3, 4, 5, 6, 7, 22, 11, 5]. However, due to the poor performance of Mahalanobis [6], Gram Matrices [7] and Rotation [22] in Table 1, we omit those three methods from the primary discussion. For completeness, we instead provide their results in Appendix E and discuss potential reasons for their failures in Appendix G. Lastly, for primary evaluations we consider holdout and Places365 images to represent the fine- and coarse-grained OOD detection tests, respectively. Note, in Appendix E we show results on additional coarse-grained datasets including Textures [42] and LSUN [43] which trend similarly to the Places365 results.

5.2 Primary detection results

Figure 5 shows the AUPR results of detecting Places365 and hold-out samples across the five benchmarks (full results including other metrics can be seen in Appendix E). Our first observation is that MixupOE consistently achieves the best detection performance against fine-grained holdout OOD samples. As shown in the bottom row of Figure 5, on the [*Bird, Dog, Flower, Car, Aircraft*] tasks MixupOE improves the AUPR by [5.5%, 4.6%, 3.6%, 6.1%, 6.0%] over MSP, and [5.8%, 4.6%, 2.1%, 8.8%, 8.0%] over vanilla OE. We re-iterate that the other detection methods provide little to no improvement over the (simple) MSP method in these fine-grained settings. Our second observation, from the top row of Figure 5, is that MixupOE can perform on par with state-of-the-art methods in detecting coarse-grained Places365 data (specifically OE and EnergyOE). This is not surprising because MixupOE’s regularization covers both the near-ID region (corresponding to fine-grained holdout images) *and* the far-ID/OOD region (corresponding to semantically unrelated images like Places365), as discussed in Section 4. Overall, these evaluation results on the five benchmarks display the effectiveness of MixupOE, particularly in fine-grained OOD detection settings.

5.3 Analysis

In this section, we perform two analyses to understand why MixupOE can improve fine-grained OOD detection performance over existing methods.

Confidence Distributions. In an effort to observe how MixupOE affects the prediction confidences, our first analysis leverages the same basic concept as in Section 3.3. Specifically, we forward pass samples from different datasets through the trained models and monitor the confidence distributions. Figure 6 shows the confidence density plots of Standard, OE, and MixupOE trained models across the five benchmarks, from which we identify two important trends. First, the MixupOE models consistently produce lower confidence predictions on holdout samples, making them more distin-

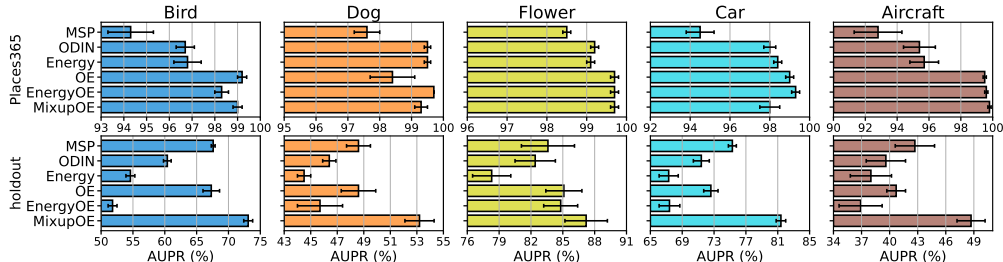


Figure 5: Detection performance (in % AUPR) for Places365 and hold-out OOD samples.

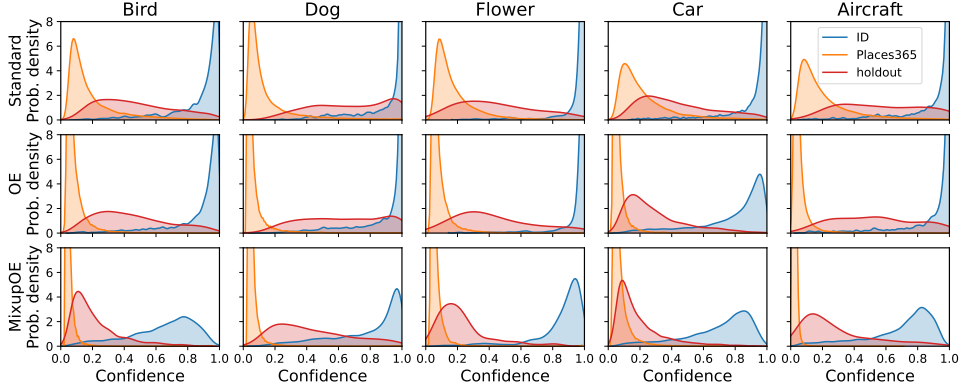


Figure 6: Confidence density plots of different input samples on the three models.

guishable from ID inputs. Second, we notice that MixupOE is generally more conservative when making predictions. Across the five benchmarks, the confidence distributions of ID, Places365, and holdout images all shift towards a lower confidence level when the model is trained with MixupOE. We believe that this behaviour results from the regularization effect of Mixup, which has shown to lead to more moderate estimates of uncertainty [21].

Saliency Maps. To interpret MixupOE’s effect from a unique perspective, we now investigate how the learned discriminative features of a MixupOE-trained model may differ from the learned features of other models. To this end, we leverage saliency maps computed w.r.t. the predicted class to qualitatively reflect which regions (features) of the input image are most important. Figure 7 shows Class Activation Mapping [44] saliency plots for several examples of both ID and OOD data as measured on the Standard, OE, and MixupOE models (see Appendix F for more). Interestingly, we find that the Standard and OE models typically pay attention to a broader (less-localized) part of the object (e.g., covering the bird’s body and the dog’s legs), while the MixupOE models focus on more restricted regions (e.g., the bird and dog’s head). This behavior is also more pronounced on the OOD data. As it relates to OOD detection performance, we suspect that MixupOE’s reliance on a smaller discriminative region (e.g., the bird’s head [45, 46, 47]) may be indicative of learning higher quality fine-grained features, which in turn may make the MixupOE model less prone to confusing fine-grained OOD samples with ID samples.

5.4 Discussion

Working with other \mathcal{D}_{out}^{OE} sets. In certain application domains, it may be difficult to collect a \mathcal{D}_{out}^{OE} set that is at all meaningful/relevant to the ID task (e.g., attempting to use animal images as \mathcal{D}_{out}^{OE} for medical image classification). In previous experiments, even though we filtered out the holdout-overlapping classes from \mathcal{D}_{out}^{OE} , some of the remaining WebVision images still had relevance to the ID tasks (e.g., despite removing dogs, the \mathcal{D}_{out}^{OE} set still contained categories of four-legged animals like cats, deer, and foxes). To evaluate the effectiveness of MixupOE when \mathcal{D}_{out}^{OE} is not at all “close” to \mathcal{D}_{in} , we now consider using the Materials in Context Database (MINC) [48] as \mathcal{D}_{out}^{OE} (which contains material images such as metal and leather). We find that on the [Bird, Dog, Flower, Car, Aircraft] tasks, MixupOE can still improve the holdout OOD AUPR by [7.0%, 3.7%, 3.6%, 6.4%, 5.3%] over

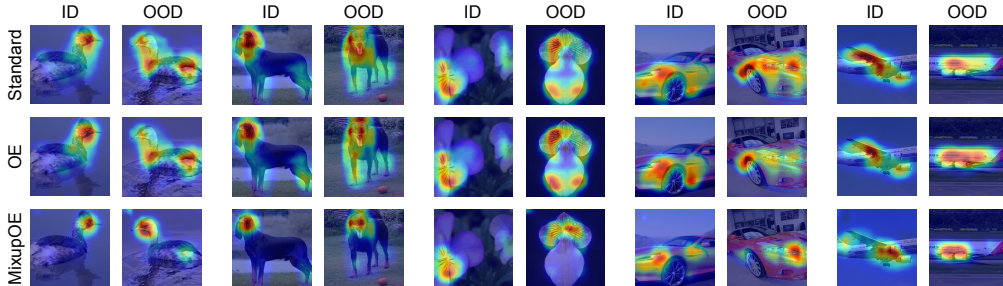


Figure 7: Saliency maps of ID/OOD inputs on the three models. From left to right, the ID/OOD examples are for Bird, Dog, Flower, Car, and Aircraft, respectively.

MSP, which is comparable to the results obtained with WebVision in Section 5.2. Thus, our key takeaway is that MixupOE can remain effective even if the $\mathcal{D}_{\text{out}}^{\text{OE}}$ set is not at all relevant to \mathcal{D}_{in} . See Appendix F for further results and discussion.

Benefits of Training MixupOE from Scratch. In previous experiments, we fine-tuned the Standard models with the OE-based objectives to save on training time. Here, we investigate whether training from scratch can lead to better performance, assuming a larger training budget is allowed. Interestingly, we find that training from scratch benefits MixupOE more than the other two OE methods (see full results in Appendix E). Across the five benchmarks, MixupOE trained from scratch provides an average increase of $\sim 1\%$ AUPR in detecting holdout images. In comparison, we find no benefit of training from scratch for OE and EnergyOE.

5.5 Coarse-grained OOD detection

Description and Setup. Although our previous experiments include Places365 to represent a coarse-grained OOD detection test, the ID tasks are all fine-grained. Recall, from our discussion of the two-axis of granularity in Section 1 that most current OOD benchmarks are also coarse-grained w.r.t. the ID classes (as shown in the top row of Figure 1). To evaluate MixupOE in a multitude of potential operational settings, our final experiment shifts to detection in fully coarse-grained environments. To enable a quality evaluation that is of similar scale and complexity to our previously constructed benchmarks, we build custom coarse-grained test environments by manually partitioning the large-scale ImageNet (INet) [49] into subsets. Concretely, we build two ID splits named INet-A and INet-B, each of which consists of 50 classes that share low granularity with each other. For each ID split, we take Textures, LSUN, Places365, and the other split as OOD data (i.e., INet-B is considered OOD w.r.t INet-A). See Appendix H.1 for additional details including the exact splits.

Notably, we make one minor adjustment to MixupOE for this setting. Observe that in MixupOE’s original design, the linear mixing coefficient λ can take values from 0 to 1, covering both far-ID and near-ID regions. However, we posit that in coarse-grained settings the OOD samples may typically be “far-away” from ID, so intuitively we may emphasize regularization over far-ID regions. Functionally, to achieve greater focus on these far-ID regions, we simply enforce that $\lambda \in [0, 0.5]$, which means that the interpolated (virtual) samples always weight the OOD samples more.

Results and Analysis. Here, we provide a summary of the most important results of this experiment and primarily focus on comparisons with OE and EnergyOE, since they are the state-of-the-art methods for coarse-grained OOD detection. See Appendix H.3 for the complete results, including comparisons with the other detection baselines. As averaged over the four OOD test sets, the AUPR performances (%) for OE / EnergyOE / MixupOE are: 51.1 / 63.0 / 54.4 on the INet-A benchmark; and 49.7 / 67.6 / 57.2 on the INet-B benchmark. Interestingly, while MixupOE provides notable AUPR increases of 3.3% and 7.5% over vanilla OE, it does not outperform EnergyOE here. We suspect this superiority of EnergyOE comes from the lack of bounds on the energy score, making it possible to achieve farther separation between ID and OOD data during training. In contrast, OE and MixupOE operate in the normalized confidence space (as defined by a softmax operation) which has an implicit lower bound of $1/\#\text{classes}$ (for OOD data) and an upper bound of 1.0 (for ID data). We posit that these tighter bounds lead to a limited range for separating the scores during training and thus lead to poorer performance in these coarse-grained tests. We leave it as future work to investigate the adaptation of MixupOE to the energy space to potentially benefit coarse-grained OOD detection.

6 Conclusion

In this work, we focus on fine-grained OOD detection, a realistic setting that considers a high granularity w.r.t. both the ID classes and the OOD data’s “closeness” to the ID data. We start by carefully building five original fine-grained OOD detection benchmarks and find that existing methods perform poorly in such fine-grained environments. We then propose a novel DNN training algorithm named Mixup Outlier Exposure, which provides a better control over the in-between region of ID and OOD by exploiting the vicinal distributions w.r.t. both inliers and outliers. Through evaluation, we demonstrate that MixupOE consistently improves fine-grained detection performance by a significant margin. We also show that MixupOE can learn high(er) quality features and remain effective even if the training outlier distribution is not relevant to ID data. We hope that this work will inspire and facilitate future research in challenging fine-grained OOD detection settings.

References

- [1] Matthias Hein, Maksym Andriushchenko, and Julian Bitterwolf. Why relu networks yield high-confidence predictions far from the training data and how to mitigate the problem. In *Proceedings of the IEEE/CVF Conference on Computer Vision and Pattern Recognition*, pages 41–50, 2019.
- [2] Abhijit Bendale and Terrance E. Boult. Towards open set deep networks. In *CVPR*, pages 1563–1572. IEEE Computer Society, 2016.
- [3] Dan Hendrycks and Kevin Gimpel. A baseline for detecting misclassified and out-of-distribution examples in neural networks. In *International Conference on Learning Representations*, 2017.
- [4] Shiyu Liang, Yixuan Li, and R Srikant. Enhancing the reliability of out-of-distribution image detection in neural networks. In *International Conference on Learning Representations*, 2018.
- [5] Weitang Liu, Xiaoyun Wang, John Owens, and Yixuan Li. Energy-based out-of-distribution detection. *Advances in Neural Information Processing Systems*, 33, 2020.
- [6] Kimin Lee, Kibok Lee, Honglak Lee, and Jinwoo Shin. A simple unified framework for detecting out-of-distribution samples and adversarial attacks. In *NeurIPS*, 2018.
- [7] Chandramouli Shama Sastry and Sageev Oore. Detecting out-of-distribution examples with gram matrices. In *International Conference on Machine Learning*, pages 8491–8501. PMLR, 2020.
- [8] Terrance DeVries and Graham W Taylor. Learning confidence for out-of-distribution detection in neural networks. *arXiv preprint arXiv:1802.04865*, 2018.
- [9] Yen-Chang Hsu, Yilin Shen, Hongxia Jin, and Zsolt Kira. Generalized odin: Detecting out-of-distribution image without learning from out-of-distribution data. In *Proceedings of the IEEE/CVF Conference on Computer Vision and Pattern Recognition*, pages 10951–10960, 2020.
- [10] Kimin Lee, Honglak Lee, Kibok Lee, and Jinwoo Shin. Training confidence-calibrated classifiers for detecting out-of-distribution samples. In *International Conference on Learning Representations*, 2018.
- [11] Dan Hendrycks, Mantas Mazeika, and Thomas Dietterich. Deep anomaly detection with outlier exposure. In *International Conference on Learning Representations*, 2018.
- [12] Nathan Inkawhich, Eric Davis, Matthew Inkawhich, Uttam Majumder, and Yiran Chen. Training sar-atr models for reliable operation in open-world environments. *IEEE Journal of Selected Topics in Applied Earth Observations and Remote Sensing*, 14:3954–3966, 2021.
- [13] Jim Winkens, Rudy Bunel, Abhijit Guha Roy, Robert Stanforth, Vivek Natarajan, Joseph R Ledsam, Patricia MacWilliams, Pushmeet Kohli, Alan Karthikesalingam, Simon Kohl, et al. Contrastive training for improved out-of-distribution detection. *arXiv preprint arXiv:2007.05566*, 2020.
- [14] Engkarat Techapanurak, Anh-Chuong Dang, and Takayuki Okatani. Bridging in-and out-of-distribution samples for their better discriminability. *arXiv preprint arXiv:2101.02500*, 2021.
- [15] Qing Li, Weidong Cai, Xiaogang Wang, Yun Zhou, David Dagan Feng, and Mei Chen. Medical image classification with convolutional neural network. In *2014 13th international conference on control automation robotics & vision (ICARCV)*, pages 844–848. IEEE, 2014.
- [16] Mengran Fan, Tapabrata Chakraborti, I Eric, Chao Chang, Yan Xu, and Jens Rittscher. Microscopic fine-grained instance classification through deep attention. In *International Conference on Medical Image Computing and Computer-Assisted Intervention*, pages 490–499. Springer, 2020.
- [17] Xiao Xiang Zhu, Devis Tuia, Lichao Mou, Gui-Song Xia, Liangpei Zhang, Feng Xu, and Friedrich Fraundorfer. Deep learning in remote sensing: A comprehensive review and list of resources. *IEEE Geoscience and Remote Sensing Magazine*, 5(4):8–36, 2017.
- [18] Gui-Song Xia, Jingwen Hu, Fan Hu, Baoguang Shi, Xiang Bai, Yanfei Zhong, Liangpei Zhang, and Xiaoqiang Lu. Aid: A benchmark data set for performance evaluation of aerial scene classification. *IEEE Transactions on Geoscience and Remote Sensing*, 55(7):3965–3981, 2017.
- [19] Gui-Song Xia, Xiang Bai, Jian Ding, Zhen Zhu, Serge Belongie, Jiebo Luo, Mihai Datcu, Marcello Pelillo, and Liangpei Zhang. Dota: A large-scale dataset for object detection in aerial images. In *Proceedings of the IEEE Conference on Computer Vision and Pattern Recognition*, pages 3974–3983, 2018.
- [20] Olivier Chapelle, Jason Weston, Léon Bottou, and Vladimir Vapnik. Vicinal risk minimization. 2001.

- [21] Hongyi Zhang, Moustapha Cisse, Yann N. Dauphin, and David Lopez-Paz. mixup: Beyond empirical risk minimization. In *International Conference on Learning Representations*, 2018.
- [22] Dan Hendrycks, Mantas Mazeika, Saurav Kadavath, and Dawn Song. Using self-supervised learning can improve model robustness and uncertainty. *Advances in Neural Information Processing Systems (NeurIPS)*, 2019.
- [23] Jihoon Tack, Sangwoo Mo, Jongheon Jeong, and Jinwoo Shin. Csi: Novelty detection via contrastive learning on distributionally shifted instances. *Advances in Neural Information Processing Systems*, 33, 2020.
- [24] Ev Zisselman and Aviv Tamar. Deep residual flow for out of distribution detection. In *Proceedings of the IEEE/CVF Conference on Computer Vision and Pattern Recognition*, pages 13994–14003, 2020.
- [25] Thomas Schlegl, Philipp Seeböck, Sebastian M Waldstein, Ursula Schmidt-Erfurth, and Georg Langs. Unsupervised anomaly detection with generative adversarial networks to guide marker discovery. In *International conference on information processing in medical imaging*, pages 146–157. Springer, 2017.
- [26] Suwon Suh, Daniel H Chae, Hyon-Goo Kang, and Seungjin Choi. Echo-state conditional variational autoencoder for anomaly detection. In *2016 International Joint Conference on Neural Networks (IJCNN)*, pages 1015–1022. IEEE, 2016.
- [27] Polina Kirichenko, Pavel Izmailov, and Andrew G Wilson. Why normalizing flows fail to detect out-of-distribution data. *Advances in Neural Information Processing Systems*, 33, 2020.
- [28] Alec Radford, Luke Metz, and Soumith Chintala. Unsupervised representation learning with deep convolutional generative adversarial networks. *arXiv preprint arXiv:1511.06434*, 2015.
- [29] Ramneet Kaur, Susmit Jha, Anirban Roy, Oleg Sokolsky, and Insup Lee. Are all outliers alike? on understanding the diversity of outliers for detecting oods. *arXiv preprint arXiv:2103.12628*, 2021.
- [30] Faruk Ahmed and Aaron Courville. Detecting semantic anomalies. In *Proceedings of the AAAI Conference on Artificial Intelligence*, volume 34, pages 3154–3162, 2020.
- [31] C. Wah, S. Branson, P. Welinder, P. Perona, and S. Belongie. The Caltech-UCSD Birds-200-2011 Dataset. Technical Report CNS-TR-2011-001, California Institute of Technology, 2011.
- [32] Ding-Nan Zou, Song-Hai Zhang, Tai-Jiang Mu, and Min Zhang. A new dataset of dog breed images and a benchmark for fine-grained classification. *Computational Visual Media*, 2020. URL <https://doi.org/10.1007/s41095-020-0184-6>.
- [33] Maria-Elena Nilsback and Andrew Zisserman. Automated flower classification over a large number of classes. In *2008 Sixth Indian Conference on Computer Vision, Graphics & Image Processing*, pages 722–729. IEEE, 2008.
- [34] Jonathan Krause, Michael Stark, Jia Deng, and Li Fei-Fei. 3d object representations for fine-grained categorization. In *4th International IEEE Workshop on 3D Representation and Recognition (3dRR-13)*, Sydney, Australia, 2013.
- [35] S. Maji, J. Kannala, E. Rahtu, M. Blaschko, and A. Vedaldi. Fine-grained visual classification of aircraft. Technical report, 2013.
- [36] Chuan Guo, Geoff Pleiss, Yu Sun, and Kilian Q Weinberger. On calibration of modern neural networks. In *International Conference on Machine Learning*, pages 1321–1330. PMLR, 2017.
- [37] Sanghyuk Chun, Seong Joon Oh, Sangdoon Yun, Dongyoon Han, Junsuk Choe, and Youngjoon Yoo. An empirical evaluation on robustness and uncertainty of regularization methods. *arXiv preprint arXiv:2003.03879*, 2020.
- [38] Bolei Zhou, Agata Lapedriza, Aditya Khosla, Aude Oliva, and Antonio Torralba. Places: A 10 million image database for scene recognition. *IEEE transactions on pattern analysis and machine intelligence*, 40(6):1452–1464, 2017.
- [39] Hongyu Guo, Yongyi Mao, and Richong Zhang. Mixup as locally linear out-of-manifold regularization. In *Proceedings of the AAAI Conference on Artificial Intelligence*, volume 33, pages 3714–3722, 2019.
- [40] Kaiming He, Xiangyu Zhang, Shaoqing Ren, and Jian Sun. Deep residual learning for image recognition. In *Proceedings of the IEEE conference on computer vision and pattern recognition*, pages 770–778, 2016.

- [41] Wen Li, Limin Wang, Wei Li, Eirikur Agustsson, and Luc Van Gool. Webvision database: Visual learning and understanding from web data. *arXiv preprint arXiv:1708.02862*, 2017.
- [42] M. Cimpoi, S. Maji, I. Kokkinos, S. Mohamed, , and A. Vedaldi. Describing textures in the wild. In *Proceedings of the IEEE Conf. on Computer Vision and Pattern Recognition (CVPR)*, 2014.
- [43] Fisher Yu, Ari Seff, Yinda Zhang, Shuran Song, Thomas Funkhouser, and Jianxiong Xiao. Lsun: Construction of a large-scale image dataset using deep learning with humans in the loop. *arXiv preprint arXiv:1506.03365*, 2015.
- [44] Bolei Zhou, Aditya Khosla, Agata Lapedriza, Aude Oliva, and Antonio Torralba. Learning deep features for discriminative localization. In *Proceedings of the IEEE conference on computer vision and pattern recognition*, pages 2921–2929, 2016.
- [45] Heliang Zheng, Jianlong Fu, Tao Mei, and Jiebo Luo. Learning multi-attention convolutional neural network for fine-grained image recognition. In *Proceedings of the IEEE international conference on computer vision*, pages 5209–5217, 2017.
- [46] Yen-Chi Hsu, Cheng-Yao Hong, Ding-Jie Chen, Ming-Sui Lee, Davi Geiger, and Tyng-Luh Liu. Fine-grained visual recognition with batch confusion norm. *arXiv preprint arXiv:1910.12423*, 2019.
- [47] Shaokang Yang, Shuai Liu, Cheng Yang, and Changhu Wang. Re-rank coarse classification with local region enhanced features for fine-grained image recognition. *arXiv preprint arXiv:2102.09875*, 2021.
- [48] Sean Bell, Paul Upchurch, Noah Snaveley, and Kavita Bala. Material recognition in the wild with the materials in context database. In *Proceedings of the IEEE conference on Computer Vision and Pattern Recognition*, pages 3479–3487, 2015.
- [49] Jia Deng, Wei Dong, Richard Socher, Li-Jia Li, Kai Li, and Li Fei-Fei. Imagenet: A large-scale hierarchical image database. In *2009 IEEE conference on computer vision and pattern recognition*, pages 248–255. Ieee, 2009.
- [50] Adam Paszke, Sam Gross, Francisco Massa, Adam Lerer, James Bradbury, Gregory Chanan, Trevor Killeen, Zeming Lin, Natalia Gimelshein, Luca Antiga, Alban Desmaison, Andreas Kopf, Edward Yang, Zachary DeVito, Martin Raison, Alykhan Tejani, Sasank Chilamkurthy, Benoit Steiner, Lu Fang, Junjie Bai, and Soumith Chintala. Pytorch: An imperative style, high-performance deep learning library. In H. Wallach, H. Larochelle, A. Beygelzimer, F. d'Alché-Buc, E. Fox, and R. Garnett, editors, *Advances in Neural Information Processing Systems 32*, pages 8024–8035. Curran Associates, Inc., 2019. URL <http://papers.neurips.cc/paper/9015-pytorch-an-imperative-style-high-performance-deep-learning-library.pdf>.
- [51] Ilya Loshchilov and Frank Hutter. Sgdr: Stochastic gradient descent with warm restarts. *arXiv preprint arXiv:1608.03983*, 2016.
- [52] Dan Hendrycks, Kimin Lee, and Mantas Mazeika. Using pre-training can improve model robustness and uncertainty. In *International Conference on Machine Learning*, pages 2712–2721. PMLR, 2019.
- [53] George A Miller. Wordnet: a lexical database for english. *Communications of the ACM*, 38(11):39–41, 1995.

A Details of the ranking mechanism for building detection benchmarks

Here we present the specific formulation of the proposed ranking mechanism which is used to guide the selection of ID classes during the construction of fine-grained OOD detection benchmarks. Given a pre-trained classifier f on all classes of the dataset, we assign a ranking score $S(c)$ to each class c , where $S(c) = \frac{1}{N_c} \sum_{i=1}^{N_c} \mathbb{1}_{y_i=c}(x_i) - \frac{1}{N_c} \sum_{i=1}^{N_c} H(f(x_i))$. Here, N_c is the number of test samples in class c , x_i is the i -th test sample of class c , $f(x_i)$ is the output softmax probability vector, $y_i = \operatorname{argmax} f(x_i)$ is the predicted category, $\mathbb{1}(\cdot)$ is the indicator function, and $H(\cdot)$ computes the entropy. In a nutshell, the first term of $S(c)$ considers the accuracy, and the second term computes the average prediction entropy. With this class-wise ranking score, we then construct the ID split using the classes on which the model is the most accurate (has the highest accuracy) and confident (has the lowest entropy/uncertainty), thus avoiding potential influences from classification accuracy and ID calibration. We re-iterate that the main purpose of such ranking procedure is to help build informative OOD detection benchmarks that more purely reflect the detection tasks' own difficulties and also to avoid the poor reproducibility of random selection as shown in Figure 2.

B Statistics of fine-grained OOD detection benchmarks

We present the number of ID classes and training samples of each fine-grained detection task in Table 3. Specifically, for the *Bird*, *Dog*, and *Car* we select 100 classes to construct the ID split. For the *Flower* and *Aircraft*, we only take 90 classes as ID since they only have around 100 classes in total. For each dataset, the remaining classes will be taken as OOD and held out from the training set. Thus, the OOD split will contain 100, 30, 12, 96, and 10 classes in the *Bird*, *Dog*, *Flower*, *Car*, and *Aircraft* test, respectively.

Table 3: Statistics of the five custom fine-grained OOD detection benchmarks

	<i>Bird</i>	<i>Dog</i>	<i>Flower</i>	<i>Car</i>	<i>Aircraft</i>
total number of classes	200	130	102	196	100
number of ID classes	100	100	90	100	90
number of ID training samples	2,999	57,035	5,878	4,162	6,000

C OOD detection evaluation setup

We employ three well-established metrics for OOD detection: false positive rate at 95% true positive rate (FPR95), area under the receiver operating characteristic curve (AUROC), and area under the precision-recall curve (AUPR). Following [3, 11], we take OOD samples as positive and ID samples as negative. Correspondingly, a lower FPR95 is better since it indicates a lower probability that an ID sample raises a false alarm when 95% of anomalies are detected. For both AUROC and AUPR, the larger the better. In the main body of this paper, we take AUPR as the major metric since it more accurately reflects performance by taking into account the base rate of anomalies [3, 11]. Also following [3, 11], the base rate between ID and OOD samples is set to 5:1 during the evaluation.

D Training and implementation details

We include additional training and implementation details that are necessary for reproducing the results. Note, in this section we primarily discuss those related to the fine-grained OOD detection experiments. See Appendix H.2 for details regarding the custom ImageNet coarse-grained setting that is discussed in Section 5.5. All experiments in this paper are conducted using PyTorch [50] with two Quadro RTX 6000 GPUs. It is also worthy to note that the training of each method is repeated five times with independent random seeds, so the results reported are all averaged over five runs.

D.1 Training setup

There are three types of training procedure involved in the experiments: standard training (used for post-training scorers including MSP [3], ODIN [4], Energy [5], Mahalanobis [6], and Gram Matrices

[7]); rotation-based self-supervised training [22] (referred to as Rotation in the main paper); and OE-based training (including OE [11], EnergyOE [5], and the proposed MixupOE). We describe useful details for each of them below.

For standard training, we train models by minimizing the vanilla cross-entropy loss over ID training data. We train for 60 epochs on the *Bird*, *Car*, and *Aircraft* dataset, and for 30 epochs on the *Flower* and *Dog* dataset to save on training time. We use the cosine learning rate scheduler [51] with an initial learning rate of 0.001, and the batch size is set to 32. One thing worthy to note here is that we initialize models with ImageNet pre-trained weights (which are available in the torchvision model zoo [50]). Otherwise, we find that the training would be too difficult to achieve reasonable accuracy, probably due to that only a small amount of training samples are contained in the fine-grained datasets (see Appendix B). Pre-training is known to be helpful for (coarse-grained) OOD detection [52], which partially explains why one can already observe a pretty good detection performance (e.g., over 90% of AUPR) against coarse-grained OOD data even with the basic MSP in Table 1. However, essentially we do not see anything inappropriate in adopting pre-training.

For rotation-based self-supervised training, we follow the objective formulated in [22]. The setup is mostly the same as for the standard training. The only difference is that we reduce the batch size to 16 so that the extra rotated images used during the training can still fit into the GPU memory.

For OE-based training, we by default fine-tune the standard models with OE/EnergyOE/MixupOE objective for 10 epochs so that only minimal extra computation is introduced. The fine-tuning also adopts cosine learning rate schedule with the learning rate being 0.001. When training from scratch, we follow the setup for standard training. Regardless of the specific objective, we use 32 as the batch size of outliers (i.e., the samples drawn from $\mathcal{D}_{\text{out}}^{\text{OE}}$) which fits within our GPU’s memory.

Lastly, unlike much previous work that primarily focus on low-resolution inputs (e.g., 32×32 CIFAR-10 images), we consider high-resolution inputs with large data dimensionality in our experiments. Specifically, the images are resized to 512×512 and then cropped to 448×448 before sent into the model.

D.2 Implementation details of scoring mechanisms

We implement most of the scoring mechanisms by following their original design/implementation. Yet, we do make a few modifications to some of the methods due to efficiency reasons.

First, ODIN and Mahalanobis incorporate input pre-processing to further make ID and OOD samples distinguishable. We omit this component in our implementation because we find its improvement relatively marginal compared with the methods’ essential component (e.g., the temperature scaling for ODIN), while introducing extra computational cost for the inference which is not negligible due to the backward pass required during the input pre-processing.

Second, for feature-based approaches Mahalanobis and Gram Matrices, we only use the feature maps of each residual block in the ResNets as the inputs to their algorithms. Otherwise, especially under a high data dimensionality that we consider in this work (512×512 px spatial resolution), the original design of computing over each single conv layer’s outputs would make the evaluation unaffordably time-consuming. Meanwhile, following [9], we aggregate the Mahalanobis scores by simply taking the summation instead of learning a weighted combination tailored to each $\mathcal{D}_{\text{out}}^{\text{test}}$.

D.3 Hyperparameters

Following [11], we use a group of validation outlier sets $\mathcal{D}_{\text{out}}^{\text{val}}$ for hyperparameter tuning of each method. We consider several types of synthetic noisy images, including *Gaussian*, *Rademacher*, and *Blobs* noises. The other $\mathcal{D}_{\text{out}}^{\text{val}}$ data are generated by corrupting the ID data. The corruption operations include computing *arithmetic mean* or *geometric mean* of random pairs of ID images, applying *speckle noise*, *inverting* the color channels, and *pixelating* the ID images. The hyperparameters are then determined such that the OOD detection performance is maximized on $\mathcal{D}_{\text{out}}^{\text{val}}$, while the ID classification accuracy is minimally affected. We first list the specific hyperparameter values used each of the methods below.

- For ODIN and Energy, we use 1000 and 1 as the temperature, respectively. These two values are also the recommended one in their original papers.

Table 4: Detection performance (in % AUPR) of MixupOE on the *Bird* dataset w.r.t. $\alpha_{\text{in-out}}$ and $\beta_{\text{in-out}}$. The number before and after the slash is for $\mathcal{D}_{\text{out}}^{\text{test}}=\text{Places365}$ and $\mathcal{D}_{\text{out}}^{\text{test}}=\text{holdout}$, respectively.

$\beta_{\text{in-out}}$ \backslash $\alpha_{\text{in-out}}$	0.5	1.0	5.0
0.4	96.7 \pm 1.0 / 69.0 \pm 0.1	97.6 \pm 0.5 / 69.4 \pm 0.4	98.8 \pm 0.2 / 71.9 \pm 0.9
1.0	96.8 \pm 0.6 / 69.7 \pm 0.9	97.5 \pm 0.7 / 70.0 \pm 0.9	99.0 \pm 0.2 / 72.7 \pm 0.4
2.0	96.4 \pm 1.0 / 70.0 \pm 0.6	97.4 \pm 0.8 / 71.0 \pm 0.6	98.2 \pm 0.5 / 72.6 \pm 0.4

- For OE (equation (1)), we use $\beta = 5.0$ for *Bird*, *Flower*, *Car*, and *Aircraft*, and use $\beta = 1.0$ for *Dog*. We do not apply a larger β to *Dog* since it will lead to a more noticeable decrease in ID accuracy. This is probably due to that the *Dog* model are exposed to much more outlier samples than others (the number of outliers encountered during the training is proportional to the number of ID training samples), and thus the regularization effect of OE is already strong with a small β in the *Dog* case.
- For EnergyOE, we refer to the hyperparameters by the symbols used in its original paper [5] for clarity. Across all the five benchmarks, we set the energy thresholds m_{in} and m_{out} to -15 and -5 , respectively, and the weighting factor λ we use is 0.1 .
- For MixupOE, we use $\alpha_{\text{in-out}} = 1.0$ across all benchmarks. As to the weighting factor $\beta_{\text{in-out}}$, similar to OE, we use 5.0 for *Bird*, *Flower*, *Car*, and *Aircraft*, and use 1.0 for *Dog*.

We further discuss how the hyperparameters can affect MixupOE. We show MixupOE’s detection performance on the *Bird* dataset w.r.t. $\alpha_{\text{in-out}}$ and $\beta_{\text{in-out}}$ in Table 4. Recall from Table 1 that the corresponding detection AUPR of MSP (against Places365 / holdout) is $94.3 / 67.6$. Apparently, MixupOE leads to consistent improvement over MSP across a wide range of $\alpha_{\text{in-out}}$ and $\beta_{\text{in-out}}$ values, indicating that MixupOE is not extremely sensitive to either of the hyperparameters. Further, we find that the effect of both hyperparameters are quite interpretable. First, a larger $\beta_{\text{in-out}}$ that weights more the “ID-OOD” term in equation (3) is indeed preferable. Second, the “optimal” $\alpha_{\text{in-out}}$ can also be well interpreted. To see this, we first show in Figure 8 the distribution of linear coefficient λ w.r.t. $\alpha_{\text{in-out}}$. It can be seen that, when $\alpha_{\text{in-out}}$ takes a smaller value (e.g., 0.4), the sampled λ will concentrate more at 0.0 and 1.0 , and in turn the vicinal distribution $\mathcal{D}_{\text{in-out}}$ will often degenerate to empirical distribution \mathcal{D}_{in} or $\mathcal{D}_{\text{out}}^{\text{OE}}$, only covering either ID or OOD region; when $\alpha_{\text{in-out}}$ takes a larger value (e.g., 2.0), the λ will touch more on intermediate values, and thus the $\mathcal{D}_{\text{in-out}}$ will characterize more the in-between region of ID and OOD. As a result, a smaller $\alpha_{\text{in-out}}$ is better at detecting “far” OOD like Places365, while a larger $\alpha_{\text{in-out}}$ helps more on detecting holdout OOD samples that are “nearer” to ID region. It is not surprising then that $\alpha_{\text{in-out}} = 1.0$, which uniformly samples λ from 0.0 to 1.0 , can lead to superior performance on both Places365 and holdout OOD as shown in Table 4. Overall, we demonstrate that MixupOE is generally effective regardless of the specific hyperparameter values, and we provide interpretation/heuristics for each of the two hyperparameters which may be helpful for tuning MixupOE on other datasets.

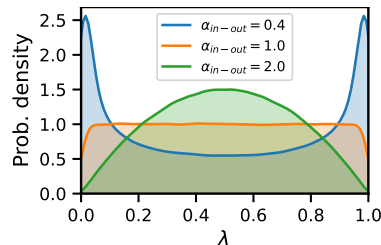


Figure 8: Distribution of the linear coefficient λ w.r.t. $\alpha_{\text{in-out}}$.

E Full results for fine-grained OOD detection

We present the full results for primary experiments of fine-grained OOD detection. Table 5 shows comprehensive evaluation results w.r.t. benchmarks, evaluation metrics, methods, and test OOD distributions. Table 5 is also the source of Table 1 and Figure 5 in the main paper. We also show the ID test accuracies of all methods on each benchmark dataset in Table 6.

Interestingly, we find that MixupOE can benefit the fine-grained classification accuracy. As averaged over five datasets, MixupOE improves the accuracy by $\sim 0.4\%$ over the standard training. When training from scratch, a larger increase of $\sim 0.8\%$ can be observed. In comparison, we find that other training dynamics do not present clear or consistent gains in accuracy.

Table 5: Full detection results in the fine-grained OOD setting. Notation = FPR95↓ / AUROC↑ / AUPR↑. * implies the implementation does not exactly follow the original design. The \mathcal{D}_{out}^{OE} used here is WebVision.

\mathcal{D}_{in}	Method	\mathcal{D}_{out}^{test}			
		Textures	LSUN	Places365	holdout
Bird	MSP [3]	7.9±0.7 / 98.2±0.2 / 94.4±0.4	3.1±1.0 / 99.4±0.2 / 97.3±0.7	7.2±1.5 / 98.6±0.3 / 94.3±1.0	34.1±1.0 / 91.4±0.2 / 67.6±0.3
	ODIN* [4]	5.6±0.6 / 98.5±0.2 / 95.7±0.4	1.1±0.3 / 99.8±0.1 / 98.8±0.3	3.3±0.5 / 99.3±0.1 / 96.7±0.4	47.2±2.7 / 88.3±0.4 / 60.4±0.6
	Energy [5]	6.1±0.8 / 98.4±0.2 / 95.6±0.3	0.8±0.3 / 99.8±0.1 / 99.0±0.3	3.1±0.5 / 99.3±0.1 / 96.8±0.6	50.5±2.9 / 86.5±0.5 / 54.6±0.7
	Mahalanobis* [6]	1.3±0.1 / 99.7±0.0 / 98.8±0.0	3.1±0.2 / 99.1±0.1 / 93.7±0.5	5.8±0.3 / 98.5±0.1 / 91.0±0.5	73.5±1.3 / 66.9±0.7 / 24.0±0.3
	Gram Matrices* [7]	1.4±0.1 / 99.4±0.1 / 95.3±0.7	3.6±0.8 / 99.0±0.3 / 91.6±2.5	7.4±1.1 / 98.2±0.3 / 88.6±1.9	56.8±1.5 / 83.7±0.4 / 50.7±1.1
	Rotation [22]	2.9±0.7 / 98.6±0.3 / 86.8±2.3	3.4±0.9 / 98.2±0.6 / 80.5±4.2	4.3±1.6 / 98.1±0.6 / 82.0±4.0	53.4±5.3 / 83.8±1.0 / 42.9±1.5
	OE (<i>fine-tune</i>) [11]	1.0±0.3 / 99.7±0.1 / 99.0±0.2	0.4±0.1 / 99.9±0.0 / 99.6±0.1	0.7±0.2 / 99.8±0.0 / 99.2±0.2	29.3±2.3 / 92.2±0.4 / 67.3±1.3
	EnergyOE (<i>fine-tune</i>) [5]	1.8±0.2 / 99.4±0.1 / 98.3±0.2	0.5±0.1 / 99.9±0.0 / 99.4±0.1	1.6±0.4 / 99.6±0.1 / 98.3±0.3	55.2±3.7 / 85.2±0.7 / 51.8±0.7
	MixupOE (<i>fine-tune</i>)	0.8±0.1 / 99.8±0.0 / 99.3±0.1	0.4±0.1 / 99.9±0.0 / 99.6±0.1	0.9±0.2 / 99.8±0.0 / 99.0±0.2	29.0±1.2 / 93.3±0.2 / 73.1±0.7
	OE (<i>scratch</i>) [11]	1.3±0.4 / 99.7±0.0 / 98.8±0.2	0.1±0.0 / 100.0±0.0 / 99.8±0.0	0.4±0.1 / 99.9±0.0 / 99.5±0.1	30.8±0.5 / 91.9±0.3 / 67.6±0.7
	EnergyOE (<i>scratch</i>) [5]	2.0±2.0 / 99.2±0.5 / 98.0±1.0	0.1±0.1 / 100.0±0.0 / 99.9±0.1	0.2±0.2 / 99.9±0.1 / 99.7±0.2	63.6±2.0 / 80.3±0.9 / 40.9±1.5
	MixupOE (<i>scratch</i>)	1.3±0.2 / 99.7±0.0 / 98.7±0.1	1.3±0.6 / 99.7±0.2 / 98.4±0.9	2.5±0.7 / 99.4±0.2 / 97.0±1.1	22.9±0.4 / 94.1±0.2 / 75.3±0.6
Dog	MSP [3]	34.3±1.5 / 93.5±0.2 / 84.3±0.6	1.6±0.6 / 99.5±0.1 / 98.4±0.3	3.5±1.0 / 99.2±0.2 / 97.6±0.4	56.8±1.0 / 82.7±0.2 / 48.6±0.9
	ODIN* [4]	22.2±1.8 / 96.2±0.1 / 91.5±0.3	0.2±0.0 / 100.0±0.0 / 99.8±0.1	0.3±0.1 / 99.8±0.0 / 99.4±0.1	70.3±2.0 / 81.5±0.4 / 46.4±0.5
	Energy [5]	22.2±2.0 / 96.2±0.2 / 91.9±0.4	0.1±0.0 / 100.0±0.0 / 99.9±0.0	0.2±0.1 / 99.9±0.0 / 99.5±0.1	71.0±1.8 / 80.9±0.3 / 44.5±0.5
	Mahalanobis* [6]	8.3±0.6 / 98.3±0.1 / 95.2±0.1	75.7±1.4 / 70.2±1.3 / 29.3±1.1	77.2±1.9 / 69.6±1.3 / 31.1±1.1	82.2±0.3 / 64.7±0.2 / 23.6±0.2
	Gram Matrices* [7]	5.4±1.0 / 98.8±0.2 / 96.0±0.6	17.8±4.7 / 97.0±0.7 / 91.3±1.7	19.5±2.6 / 96.7±0.4 / 91.2±1.3	82.8±0.8 / 72.1±0.3 / 35.2±0.3
	Rotation [22]	14.0±6.2 / 96.8±1.3 / 86.5±5.4	1.5±0.8 / 99.3±0.4 / 92.7±3.9	2.2±1.0 / 99.0±0.4 / 92.0±4.3	69.8±1.9 / 79.6±0.5 / 42.1±1.5
	OE (<i>fine-tune</i>) [11]	27.7±11.0 / 95.1±2.0 / 88.2±4.6	1.0±1.2 / 99.7±0.2 / 98.9±0.7	1.9±1.5 / 99.5±0.2 / 98.4±0.7	58.1±1.3 / 82.8±0.4 / 49.6±1.3
	EnergyOE (<i>fine-tune</i>) [5]	3.8±2.0 / 98.8±0.4 / 97.3±0.9	0.0±0.1 / 100.0±0.0 / 99.9±0.1	0.1±0.1 / 99.9±0.0 / 99.7±0.0	67.0±4.0 / 81.1±0.9 / 45.7±1.7
	MixupOE (<i>fine-tune</i>)	9.5±3.0 / 98.0±0.5 / 94.4±1.1	0.2±0.1 / 99.9±0.0 / 99.6±0.2	0.3±0.2 / 99.8±0.0 / 99.3±0.2	54.9±1.3 / 84.9±0.3 / 53.2±1.1
	OE (<i>scratch</i>) [11]	29.9±5.6 / 94.7±1.1 / 87.3±2.4	1.1±4.0 / 99.6±0.2 / 98.7±0.5	2.5±1.5 / 99.4±0.2 / 98.1±0.6	58.7±2.0 / 82.7±0.4 / 48.4±0.9
	EnergyOE (<i>scratch</i>) [5]	21.5±6.7 / 96.5±0.7 / 92.9±1.1	0.1±0.0 / 100.0±0.0 / 99.9±0.0	0.2±0.0 / 99.8±0.0 / 99.5±0.1	72.1±3.8 / 77.0±1.4 / 38.8±2.3
	MixupOE (<i>scratch</i>)	9.0±3.2 / 98.1±0.6 / 94.1±1.5	0.2±0.1 / 99.9±0.0 / 99.7±0.1	0.4±0.1 / 99.8±0.0 / 99.3±0.2	56.5±3.4 / 84.7±0.8 / 52.6±2.2
Flower	MSP [3]	5.7±0.8 / 98.8±0.2 / 95.1±0.6	0.8±0.3 / 99.9±0.0 / 99.4±0.2	2.1±0.1 / 99.7±0.0 / 98.5±0.1	10.1±1.0 / 97.7±0.4 / 83.6±2.5
	ODIN* [4]	5.5±0.9 / 99.0±0.1 / 96.4±0.4	0.3±0.1 / 100.0±0.0 / 99.8±0.1	0.9±0.1 / 99.8±0.0 / 99.2±0.1	11.8±1.6 / 97.1±0.3 / 82.4±1.9
	Energy [5]	5.7±0.8 / 98.9±0.2 / 96.3±0.4	0.2±0.0 / 100.0±0.0 / 99.8±0.1	0.9±0.2 / 99.8±0.0 / 99.1±0.1	12.9±0.7 / 96.6±0.3 / 78.3±1.8
	Mahalanobis* [6]	0.3±0.1 / 99.9±0.0 / 99.8±0.0	1.4±0.2 / 99.7±0.0 / 98.3±0.3	1.6±0.2 / 99.6±0.1 / 97.6±0.3	48.6±1.3 / 84.7±0.2 / 43.5±0.4
	Gram Matrices* [7]	1.1±0.2 / 99.7±0.0 / 97.5±0.6	1.4±0.3 / 99.5±0.1 / 95.1±0.6	1.8±0.3 / 99.4±0.1 / 94.8±0.7	12.3±1.7 / 96.1±0.2 / 69.2±2.4
	Rotation [22]	19.3±1.9 / 91.7±0.9 / 55.4±2.7	14.4±1.0 / 91.2±0.7 / 50.7±2.2	16.7±0.9 / 90.3±0.5 / 48.4±1.2	35.5±6.4 / 85.4±0.9 / 32.5±2.1
	OE (<i>fine-tune</i>) [11]	2.6±0.6 / 99.6±0.1 / 98.3±0.5	0.1±0.1 / 100.0±0.0 / 99.8±0.1	0.3±0.1 / 99.9±0.0 / 99.7±0.1	9.6±2.2 / 97.9±0.3 / 85.1±1.7
	EnergyOE (<i>fine-tune</i>) [5]	1.5±0.5 / 99.7±0.1 / 98.9±0.3	0.0±0.0 / 100.0±0.0 / 99.9±0.0	0.2±0.1 / 99.9±0.0 / 99.7±0.1	13.7±4.0 / 97.2±0.6 / 84.8±1.6
	MixupOE (<i>fine-tune</i>)	1.8±0.2 / 99.6±0.1 / 98.5±0.3	0.5±0.3 / 99.9±0.0 / 99.6±0.2	0.4±0.3 / 99.9±0.0 / 99.7±0.1	5.7±1.2 / 98.3±0.2 / 87.2±2.0
	OE (<i>scratch</i>) [11]	2.7±0.7 / 99.5±0.2 / 98.2±0.5	0.1±0.1 / 100.0±0.0 / 99.9±0.1	0.2±0.1 / 99.9±0.0 / 99.8±0.0	12.5±3.7 / 97.4±0.3 / 83.9±2.5
	EnergyOE (<i>scratch</i>) [5]	2.6±0.8 / 99.3±0.1 / 98.1±0.3	0.0±0.0 / 100.0±0.0 / 100.0±0.0	0.1±0.1 / 99.9±0.0 / 99.8±0.0	32.9±5.9 / 92.5±1.0 / 61.9±3.8
	MixupOE (<i>scratch</i>)	2.0±0.4 / 99.6±0.1 / 98.5±0.3	0.6±0.2 / 99.9±0.0 / 99.4±0.1	0.6±0.2 / 99.9±0.0 / 99.4±0.2	7.9±2.0 / 98.3±0.3 / 87.9±1.5
Car	MSP [3]	7.3±1.7 / 98.6±0.3 / 95.1±1.1	5.9±1.2 / 98.9±0.2 / 95.2±0.9	6.7±0.8 / 98.6±0.2 / 94.5±0.7	21.9±1.5 / 94.0±0.2 / 75.3±0.5
	ODIN* [4]	4.5±1.4 / 98.9±0.2 / 96.9±0.7	1.7±0.3 / 99.7±0.1 / 98.5±0.3	2.2±0.4 / 99.5±0.1 / 98.0±0.3	30.5±2.3 / 92.4±0.3 / 71.4±1.0
	Energy [5]	4.5±1.2 / 98.8±0.2 / 97.0±0.6	1.1±0.3 / 99.8±0.0 / 99.0±0.2	1.7±0.3 / 99.5±0.1 / 98.4±0.2	32.5±2.0 / 91.5±0.4 / 67.3±1.2
	Mahalanobis* [6]	0.1±0.0 / 100.0±0.0 / 99.8±0.0	14.1±0.3 / 95.3±0.1 / 72.8±0.5	14.6±0.6 / 95.8±0.1 / 78.3±0.3	72.7±2.0 / 68.1±0.4 / 25.0±0.2
	Gram Matrices* [7]	0.6±0.1 / 99.8±0.1 / 98.2±0.7	3.9±1.0 / 99.0±0.2 / 93.0±1.3	3.7±0.6 / 99.0±0.2 / 93.6±1.5	51.9±1.9 / 86.2±0.5 / 54.9±0.5
	Rotation [22]	0.0±0.0 / 100.0±0.0 / 99.9±0.0	0.4±0.2 / 99.9±0.0 / 99.5±0.2	0.1±0.0 / 99.9±0.0 / 99.7±0.1	28.7±2.0 / 92.4±0.4 / 77.8±0.8
	OE (<i>fine-tune</i>) [11]	0.6±0.3 / 99.8±0.1 / 99.2±0.2	0.6±0.2 / 99.9±0.0 / 99.3±0.1	1.0±0.3 / 99.7±0.1 / 99.0±0.2	24.8±1.8 / 93.4±0.4 / 72.6±0.9
	EnergyOE (<i>fine-tune</i>) [5]	0.0±0.0 / 99.9±0.1 / 99.8±0.1	0.3±0.2 / 99.9±0.0 / 99.6±0.2	0.5±0.2 / 99.8±0.1 / 99.3±0.2	34.6±2.6 / 91.3±0.4 / 67.4±1.3
	MixupOE (<i>fine-tune</i>)	0.8±0.3 / 99.6±0.1 / 98.9±0.2	0.9±0.5 / 99.8±0.1 / 99.1±0.4	1.9±0.5 / 99.6±0.1 / 98.0±0.5	18.2±0.8 / 95.5±0.2 / 81.4±0.6
	OE (<i>scratch</i>) [11]	0.6±0.2 / 99.7±0.0 / 99.1±0.1	0.9±0.4 / 99.8±0.1 / 99.2±0.3	1.1±0.6 / 99.7±0.1 / 99.0±0.4	25.9±2.2 / 93.2±0.5 / 72.0±1.8
	EnergyOE (<i>scratch</i>) [5]	0.9±0.4 / 99.3±0.2 / 98.6±0.3	0.2±0.2 / 99.9±0.0 / 99.6±0.2	0.7±0.5 / 99.8±0.1 / 99.0±0.5	53.1±8.0 / 83.8±3.5 / 47.1±6.3
	MixupOE (<i>scratch</i>)	1.0±0.2 / 99.7±0.1 / 99.0±0.1	1.1±0.4 / 99.8±0.1 / 98.8±0.4	2.1±0.5 / 99.5±0.1 / 97.4±0.6	15.8±1.4 / 96.1±0.3 / 84.2±0.6
Aircraft	MSP [3]	15.0±1.2 / 97.0±0.3 / 89.3±1.0	9.3±2.0 / 98.0±0.4 / 91.1±1.9	8.3±1.5 / 98.3±0.4 / 92.8±1.5	51.0±5.5 / 87.5±0.7 / 42.7±2.1
	ODIN* [4]	19.6±3.5 / 95.9±0.4 / 90.0±1.1	4.0±0.8 / 98.9±0.2 / 94.3±1.2	3.8±0.7 / 99.0±0.2 / 95.4±1.0	75.1±2.5 / 83.6±1.1 / 39.6±2.1
	Energy [5]	21.8±4.2 / 95.6±0.4 / 89.9±1.2	3.9±0.8 / 99.0±0.2 / 94.8±1.1	3.6±0.6 / 99.1±0.2 / 95.7±0.9	76.4±2.1 / 82.5±1.2 / 38.0±2.2
	Mahalanobis* [6]	0.1±0.0 / 100.0±0.0 / 99.9±0.0	0.7±0.0 / 99.6±0.0 / 96.9±0.4	0.6±0.0 / 99.8±0.0 / 98.4±0.2	83.3±1.1 / 61.9±0.3 / 14.5±0.4
	Gram Matrices* [7]	0.8±0.1 / 99.7±0.0 / 97.7±0.5	2.0±0.3 / 99.3±0.1 / 93.7±0.8	1.2±0.1 / 99.6±0.1 / 96.1±0.9	71.6±2.5 / 77.6±0.6 / 27.6±1.0
	Rotation [22]	1.1±0.1 / 99.6±0.1 / 98.7±0.2	1.6±0.4 / 99.6±0.1 / 97.4±0.5	1.9±0.4 / 99.5±0.1 / 97.3±0.6	75.0±5.5 / 82.1±1.0 / 36.1±2.8
	OE (<i>fine-tune</i>) [11]	1.3±0.6 / 99.7±0.1 / 98.6±0.5	0.5±0.3 / 99.9±0.0 / 99.4±0.2	0.4±0.2 / 99.9±0.0 / 99.5±0.1	53.3±6.0 / 87.0±0.5 / 40.7±1.0
	EnergyOE (<i>fine-tune</i>) [5]	1.1±0.5 / 99.4±0.1 / 98.6±0.4	0.5±0.1 / 99.9±0.0 / 99.5±0.1	0.5±0.1 / 99.9±0.0 / 99.6±0.1	74.8±5.8 / 83.0±0.3 / 36.9±2.3
	MixupOE (<i>fine-tune</i>)	2.1±0.5 / 99.4±0.1 / 97.9±0.5	0.3±0.1 / 99.9±0.0 / 99.6±0.1	0.1±0.1 / 100.0±0.0 / 99.8±0.1	54.6±6.2 / 88.6±0.6 / 48.7±1.5
	OE (<i>scratch</i>) [11]	0.7±0.3 / 99.8±0.1 / 99.2±0.3	0.1±0.1 / 100.0±0.0 / 99.8±0.1	0.1±0.1 / 100.0±0.0 / 99.9±0.1	55.5±5.4 / 86.6±0.7 / 40.6±1.6
	EnergyOE (<i>scratch</i>) [5]	2.3±1.6 / 98.6±0.4 / 97.7±0.6	0.1±0.1 / 100.0±0.0 / 99.9±0.1	0.0±0.1 / 100.0±0.0 / 99.9±0.1	80.3±3.0 / 76.3±2.9 / 28.9±3.0
	MixupOE (<i>scratch</i>)	2.9±0.7 / 99.3±0.2 / 97.3±0.9	0.2±0.1 / 100.0±0.0 / 99.7±0.2	0.2±0.1 / 100.0±0.0 / 99.8±0.1	52.6±8.2 / 88.9±0.9 / 49.4±1.6

Table 6: Accuracies of each method on fine-grained ID test data

\mathcal{D}_{in}	Standard	Rotation [22]	OE [11]		EnergyOE [5]		MixupOE	
			fine-tune	scratch	fine-tune	scratch	fine-tune	scratch
Bird	95.0±0.2	95.0±0.2	95.4±0.2	94.9±0.1	94.1±0.2	92.6±0.6	95.7±0.2	95.9±0.2
Dog	86.2±0.2	85.4±0.3	85.7±0.4	85.8±0.2	85.9±0.1	84.7±0.6	84.8±0.4	85.4±0.3
Flower	98.3±0.1	98.5±0.2	98.4±0.1	98.3±0.1	98.2±0.4	97.4±0.2	99.2±0.1	99.5±0.1
Car	96.7±0.1	97.4±0.3	96.3±0.4	96.1±0.3	96.2±0.2	94.2±2.1	97.6±0.2	98.2±0.1
Aircraft	92.5±0.3	93.3±0.4	92.5±0.4	92.0±0.5	92.4±0.2	89.6±1.3	93.3±0.3	94.1±0.2

F Additional plots and results

In this section, we show several additional plots/results for the experiments in the main paper. First, Figure 9 shows the confidence density plots of the Standard and OE model on the *Bird*, *Flower*, *Car*, and *Aircraft* dataset, corresponding to the preliminary analysis discussed in Section 3.3. We find that they mostly present similar patterns to those in Figure 3 and Figure 4, except for the *Car* case, where the OE model surprisingly manages to improve the calibration in the “near-ID” region as evidenced by the lower confidences on both holdout and interpolated samples (see the plot in the third row and the fourth column). We suspect that this is because in this case $\mathcal{D}_{\text{out}}^{\text{OE}}$ somehow contains a few outlier samples that are naturally “close” to the car images and in turn can induce regularization over the near-ID region. However, such effect of OE is rather circumstantial and depends heavily on the “closeness” between $\mathcal{D}_{\text{out}}^{\text{OE}}$ and \mathcal{D}_{in} which cannot be guaranteed easily. In contrast, MixupOE by design provides a more controlled and effective way to regularize the model’s near-ID behaviour, which does not require $\mathcal{D}_{\text{out}}^{\text{OE}}$ to have images that can directly serve as near-ID inputs.

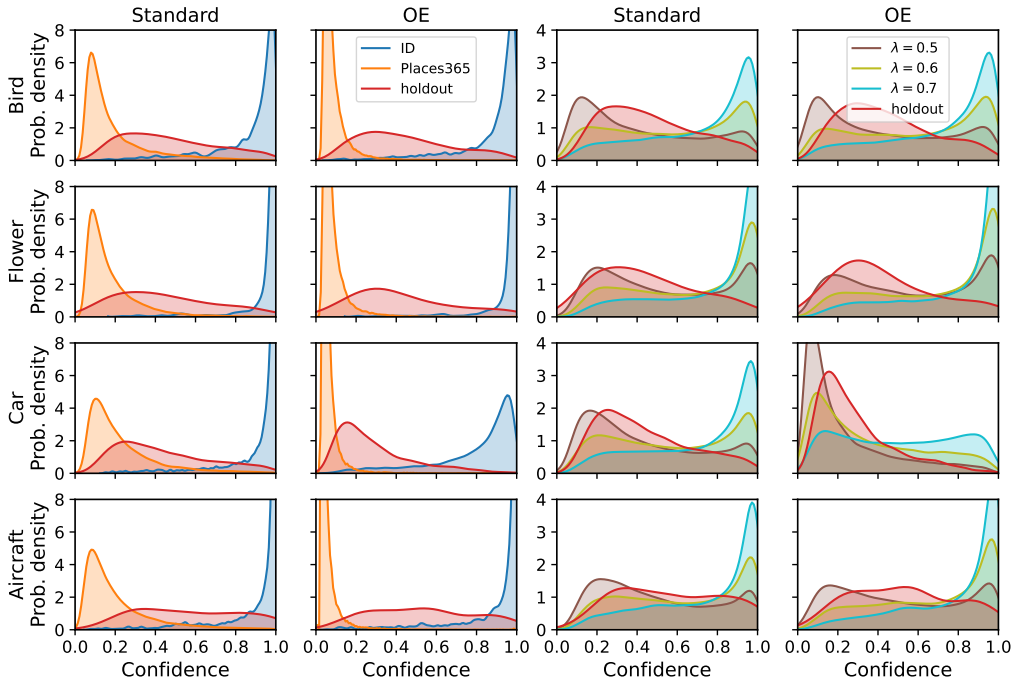


Figure 9: Additional density plots of different inputs’ confidence distributions.

Next, we show MixupOE’s performance of detecting Places365 and holdout OOD samples w.r.t. $\mathcal{D}_{\text{out}}^{\text{OE}}$ in Figure 10, which corresponds to the first discussion in Section 5.4 where we only mentioned the holdout detection results. The main takeaway from Figure 10 is that MixupOE can help detecting both coarse- and fine-grained OOD examples regardless of which exact $\mathcal{D}_{\text{out}}^{\text{OE}}$ is used. We also train OE and EnergyOE models with MINC as $\mathcal{D}_{\text{out}}^{\text{OE}}$, and find that they still cannot (consistently) detect holdout samples better than MSP, indicating that their difficulties are inherent rather than the consequences of using an “inappropriate” outlier training set.

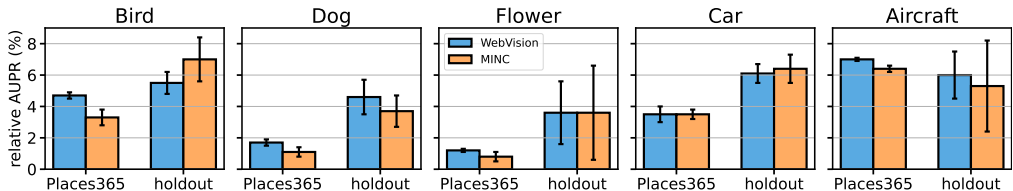


Figure 10: Relative AUPR improvement of MixupOE over MSP w.r.t. $\mathcal{D}_{\text{out}}^{\text{OE}}$.

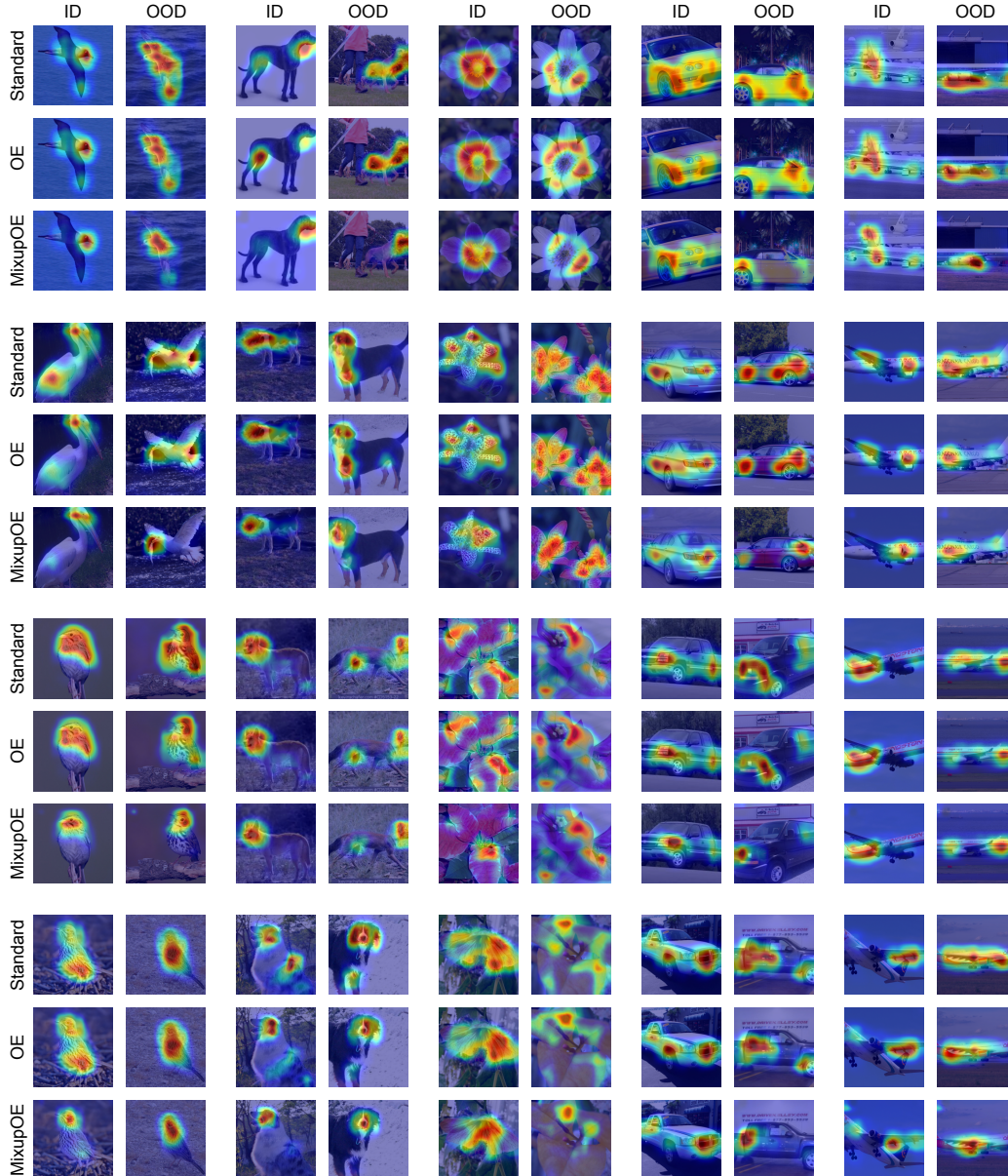


Figure 11: Additional saliency maps of ID/OOD inputs on the three models. From left to right, the ID/OOD examples are for Bird, Dog, Flower, Car, and Aircraft, respectively.

Lastly, in Figure 11 we show additional saliency maps for ID/OOD examples generated on the Standard, OE, and MixupOE model, which display similar patterns to Figure 7 in Section 5.3.

G Discussion on Mahalanobis, Gram Matrices, and Rotation

In Table 1 (or essentially, Table 5), we find that Mahalanobis, Gram Matrices, and Rotation perform poorly in detecting fine-grained OOD examples. Perhaps even more surprisingly, these three methods can also be worse than others in certain cases when facing coarse-grained OOD data (e.g., LSUN and Places365), although they have shown to be among the best in coarse-grained settings [6, 7, 22]. In this section, our goal is thus to discuss potential reasons for the conflicting trends between what have been reported by previous works and those observed in our work.

Mahalanobis and Gram Matrices. We identify two potential reasons for these two feature-based scoring mechanisms. First, although it is unclear how this can affect the detection, we note that both methods are evaluated under a low input dimensionality (i.e., 32×32) in their original works, while we are operating at a much larger scale (i.e., 448×448). Second, we find that there exists over-estimates in the reported detection rates of these methods due to the use of poor benchmark tests. Specifically, one of the primary tests in both [6] and [7] is detecting samples from a resized version of LSUN (“LSUN-r”) with a classifier trained on CIFAR-10. However, due to inappropriate resizing operations, LSUN-r images exhibit obvious artifacts [23] and might provide trivial signals for feature-based methods to exploit to achieve high detection performance. As evidence, on a pre-trained CIFAR-10 model, Gram Matrices (using its official implementation) achieves 99.8% AUROC against LSUN-r; yet, if one puts aside LSUN-r and instead resizes the LSUN images with Pytorch transformations, the AUROC of Gram Matrices immediately drops to 79.1%. By contrast, the MSP’s AUROC is 91.7% and 88.1%, respectively. We also observe similar trends in Mahalanobis’s performance. One can obviously see how the use of LSUN-r leads to over-estimated detection abilities for these two feature-based methods.

Rotation. We suspect the major “problem” with Rotation is that its effectiveness may depend on the characteristics of the considered visual objects. As evidence, according to Table 5, Rotation indeed helps detecting coarse-grained samples when the ID samples are cars and aircrafts, but not when they are birds, dogs, or flowers. This is perhaps not too surprising, since some objects are naturally “insensitive” to rotations. For example, a flower can appear similarly to its original look after rotation, which makes the signal obtained from predicting the rotation angle much less informative for distinguishing ID from OOD samples. With that being said, we also acknowledge that such hypothesis may not account well for the poor performance in the *Bird* and *Dog* case, and a more thorough study is necessary in the future.

H Coarse-grained OOD detection test

In this section, we provide additional details and results that correspond to the coarse-grained OOD detection experiments discussed in Section 5.5.

H.1 ImageNet split construction

We show in Figure 12 the ImageNet classes used to construct the two splits which serve as the ID split in the coarse-grained detection experiments. Each of the two splits consist of 50 classes. Importantly, all of the 100 classes are selected such that only a minimal level of granularity is shared across them.

H.2 Training details

Setup. We use ResNet-18 [40] as the model architecture for coarse-grained detection experiments. We train the “standard” models for 90 epochs, and perform 10 epochs of fine-tuning with the OE/EnergyOE/MixupOE objective. To save on training time, we also let Rotation adopt fine-tuning this time. Both the standard training and the fine-tuning uses cosine learning rate schedule, and the initial learning rate is 0.1 and 0.001, respectively. We set the batch size to 256 and 512 for ID samples and outlier samples, respectively. Following common practice on ImageNet, we resize images such that the smallest side has 256 pixels and then cropped them to the size 224×224 . Lastly, we again consider WebVision as the outlier training set for OE-based methods. Relevant images to INet-A/B are filtered out from WebVision based on the WordNet hierarchy [53].

Hyperparameters. For ODIN and Energy, we still use 1000 and 1 as the temperature, respectively. For OE, we use $\beta = 0.5$. For EnergyOE, we use $m_{in} = -27$, $m_{out} = -5$, and $\lambda = 0.05$. For MixupOE, we use $\alpha_{in-out} = 0.4$ and $\beta_{in-out} = 5.0$. In addition, every time $\lambda \sim \text{Beta}(\alpha_{in-out}, \alpha_{in-out})$ is sampled, we take $\lambda' = \min(\lambda, 1 - \lambda)$ as the mixing coefficient for ID samples such that the interpolated samples always weight the OOD samples more.

H.3 Full detection results

Here we present the expanded results for coarse-grained OOD detection in Table 7. We further show the ID accuracy results of each method in Table 8.

INet-A			INet-B		
class id	class wnid	class name	class id	class wnid	class name
933	n07697313	cheeseburger	589	n03483316	hand blower
404	n02690373	airliner	696	n03876231	paintbrush
805	n04254680	soccer ball	902	n04579432	whistle
920	n06874185	traffic light	701	n03888257	parachute
954	n07753592	banana	851	n04404412	television
953	n07753275	pineapple	491	n03000684	chain saw
949	n07745940	strawberry	512	n03109150	bottle screw
796	n04229816	ski mask	621	n03649909	lawn mower
963	n07873807	pizza, pizza pie	950	n07747607	orange
721	n03938244	pillow	937	n07714990	broccoli
550	n03297495	espresso maker	974	n09288635	geyser
340	n02391049	zebra	973	n09256479	coral reef
679	n03814906	necklace	776	n04141076	saxophone
658	n03775071	mitten	846	n04380533	table lamp
51	n01704323	triceratops	575	n03445924	golfcart
629	n03676483	lipstick	763	n04086273	six-gun
713	n03924679	photocopier	531	n03197337	digital watch
896	n04553703	washbasin	488	n02999410	chain
767	n04116512	rubber eraser	743	n04005630	prison
514	n03124043	cowboy boot	645	n03733131	maypole
697	n03877472	pajama	535	n03208938	disk brake
838	n04357314	sunscreen	412	n02747177	trash can
437	n02814860	lighthouse	635	n03706229	magnetic compass
522	n03134739	croquet ball	987	n12144580	corn
665	n03785016	moped	948	n07742313	Granny Smith
413	n02749479	assault rifle	812	n04266014	space shuttle
596	n03498962	hatchet	977	n09421951	sandbar
785	n04162706	seat belt	430	n02802426	basketball
398	n02666196	abacus	605	n03584254	iPod
604	n03544143	hourglass	836	n04355933	sunglass
917	n06596364	comic book	150	n02077923	sea lion
966	n07892512	red wine	539	n03223299	doormat
804	n04254120	soap dispenser	647	n03733805	measuring cup
905	n04590129	window shade	477	n02966687	carpenter's kit
756	n04049303	rain barrel	910	n04597913	wooden spoon
971	n09229709	bubble	693	n03873416	paddle
540	n03240683	drilling platform	999	n15075141	toilet tissue
719	n03935335	piggy bank	496	n03026506	Christmas stocking
752	n04039381	racket	924	n07583066	guacamole
919	n06794110	street sign	927	n07613480	trifle
419	n02786058	band aid	903	n04584207	wig
932	n07695742	pretzel	652	n03763968	military uniform
926	n07590611	hot pot	922	n07565083	menu
982	n10148035	groom	930	n07684084	French loaf
863	n04458633	totem pole	578	n03450230	gown
868	n04476259	tray	925	n07584110	consomme
584	n03476684	hair slide	733	n03976657	pole
592	n03492542	hard disk	967	n07920052	espresso
769	n04118776	rule	830	n04336792	stretcher
545	n03271574	electric fan	959	n07831146	carbonara

Figure 12: Construction of INet-A/B splits used in coarse-grained OOD detection tests.

Table 7: Full detection results in the coarse-grained OOD setting. Notation = FPR95 \downarrow / AUROC \uparrow / AUPR \uparrow . * implies the implementation does not exactly follow the original design. The $\mathcal{D}_{\text{out}}^{\text{OE}}$ used here is WebVision. OE-based methods here adopt fine-tuning.

\mathcal{D}_{in}	Method	$\mathcal{D}_{\text{out}}^{\text{test}}$			
		Textures	LSUN	Places365	INet-B/A
INet-A	MSP [3]	49.3 \pm 1.2 / 83.2 \pm 0.5 / 48.9 \pm 2.0	49.9 \pm 1.5 / 80.4 \pm 0.5 / 38.0 \pm 1.5	44.3 \pm 1.1 / 83.4 \pm 0.3 / 43.8 \pm 1.3	48.5 \pm 0.7 / 81.4 \pm 0.4 / 39.8 \pm 1.3
	ODIN* [4]	46.8 \pm 2.0 / 86.1 \pm 0.6 / 58.1 \pm 1.5	48.3 \pm 1.4 / 81.7 \pm 0.5 / 38.8 \pm 1.4	42.2 \pm 1.1 / 85.1 \pm 0.4 / 45.4 \pm 1.2	50.6 \pm 1.0 / 81.7 \pm 0.4 / 40.9 \pm 1.2
	Energy [5]	47.0 \pm 1.9 / 86.3 \pm 0.6 / 59.8 \pm 1.0	48.3 \pm 1.4 / 81.5 \pm 0.5 / 38.1 \pm 1.1	42.1 \pm 1.2 / 84.9 \pm 0.3 / 44.6 \pm 0.9	50.7 \pm 1.2 / 81.5 \pm 0.4 / 40.5 \pm 0.9
	Mahalanobis* [6]	47.9 \pm 1.8 / 89.9 \pm 0.3 / 71.4 \pm 0.5	94.5 \pm 0.4 / 41.6 \pm 0.5 / 13.2 \pm 0.1	94.9 \pm 0.5 / 42.9 \pm 1.0 / 13.7 \pm 0.3	94.5 \pm 0.3 / 47.3 \pm 0.5 / 15.4 \pm 0.3
	Gram Matrices* [7]	41.7 \pm 3.3 / 93.3 \pm 0.3 / 84.5 \pm 0.3	98.1 \pm 2.1 / 59.0 \pm 0.6 / 23.0 \pm 0.5	98.1 \pm 1.7 / 62.8 \pm 0.3 / 28.3 \pm 0.3	99.3 \pm 0.9 / 62.6 \pm 0.3 / 28.7 \pm 0.4
	Rotation [22]	41.2 \pm 2.0 / 88.6 \pm 0.6 / 64.9 \pm 1.1	52.3 \pm 1.1 / 78.8 \pm 0.5 / 33.1 \pm 0.8	48.1 \pm 0.6 / 81.7 \pm 0.3 / 38.6 \pm 0.5	53.2 \pm 0.8 / 80.5 \pm 0.2 / 38.6 \pm 0.6
	OE [11]	48.3 \pm 1.0 / 85.0 \pm 0.6 / 56.0 \pm 2.8	43.5 \pm 1.3 / 84.9 \pm 1.0 / 48.6 \pm 3.3	37.5 \pm 1.0 / 88.3 \pm 0.5 / 57.6 \pm 1.7	49.0 \pm 0.8 / 82.4 \pm 0.5 / 42.2 \pm 0.9
	EnergyOE [5]	51.0 \pm 1.9 / 85.7 \pm 0.2 / 58.0 \pm 1.1	32.9 \pm 2.7 / 91.5 \pm 0.7 / 69.5 \pm 2.2	21.9 \pm 0.5 / 95.1 \pm 0.3 / 81.5 \pm 1.7	51.2 \pm 1.1 / 82.3 \pm 0.5 / 43.2 \pm 1.1
	MixupOE	46.6 \pm 1.4 / 87.1 \pm 0.7 / 62.4 \pm 1.6	43.9 \pm 1.0 / 85.6 \pm 0.4 / 50.5 \pm 0.5	34.9 \pm 1.3 / 90.4 \pm 0.4 / 64.1 \pm 0.8	50.4 \pm 0.8 / 81.6 \pm 0.4 / 40.6 \pm 0.9
	INet-B	MSP [3]	44.7 \pm 1.2 / 83.3 \pm 0.4 / 46.2 \pm 0.9	44.1 \pm 0.3 / 82.4 \pm 0.2 / 40.0 \pm 0.9	48.5 \pm 1.1 / 82.0 \pm 0.2 / 41.1 \pm 0.7
ODIN* [4]		45.1 \pm 1.6 / 86.3 \pm 0.6 / 56.2 \pm 1.5	43.1 \pm 0.3 / 83.0 \pm 0.2 / 39.5 \pm 0.6	47.7 \pm 0.8 / 82.8 \pm 0.2 / 41.3 \pm 0.8	55.9 \pm 0.7 / 80.5 \pm 0.3 / 40.1 \pm 0.6
Energy [5]		45.4 \pm 1.6 / 86.5 \pm 0.6 / 58.3 \pm 1.5	43.4 \pm 0.3 / 82.7 \pm 0.2 / 38.4 \pm 0.5	47.8 \pm 0.8 / 82.5 \pm 0.3 / 40.3 \pm 0.8	56.4 \pm 0.7 / 80.2 \pm 0.3 / 39.6 \pm 0.7
Mahalanobis* [6]		48.0 \pm 2.4 / 91.1 \pm 0.2 / 76.5 \pm 0.6	91.2 \pm 0.8 / 49.9 \pm 0.3 / 15.5 \pm 0.0	93.5 \pm 0.8 / 47.9 \pm 1.1 / 15.3 \pm 0.4	92.3 \pm 0.9 / 53.9 \pm 0.5 / 19.2 \pm 0.2
Gram Matrices* [7]		52.4 \pm 0.9 / 91.6 \pm 0.2 / 82.2 \pm 0.3	100.0 \pm 0.0 / 59.6 \pm 1.1 / 23.2 \pm 0.7	100.0 \pm 0.0 / 59.6 \pm 0.7 / 25.1 \pm 0.7	100.0 \pm 0.0 / 62.0 \pm 0.9 / 28.0 \pm 1.1
Rotation [22]		41.1 \pm 2.5 / 88.4 \pm 0.6 / 62.4 \pm 1.2	46.1 \pm 0.8 / 80.7 \pm 0.6 / 34.5 \pm 0.9	53.1 \pm 1.0 / 79.5 \pm 0.6 / 35.3 \pm 1.1	56.6 \pm 1.1 / 79.8 \pm 0.2 / 38.5 \pm 0.6
OE [11]		42.4 \pm 1.3 / 85.4 \pm 0.5 / 50.2 \pm 1.8	37.5 \pm 0.5 / 87.5 \pm 0.4 / 53.2 \pm 1.3	41.3 \pm 0.9 / 86.8 \pm 0.3 / 54.0 \pm 0.9	50.0 \pm 0.5 / 82.0 \pm 0.4 / 41.6 \pm 1.3
EnergyOE [5]		45.2 \pm 0.4 / 87.8 \pm 0.4 / 63.1 \pm 1.4	22.6 \pm 1.7 / 94.9 \pm 0.5 / 80.2 \pm 1.9	20.9 \pm 2.7 / 95.7 \pm 0.6 / 84.8 \pm 2.4	59.5 \pm 0.7 / 79.8 \pm 0.5 / 42.2 \pm 0.6
MixupOE		38.3 \pm 1.1 / 89.0 \pm 0.4 / 63.2 \pm 1.9	35.9 \pm 1.4 / 88.9 \pm 1.0 / 60.2 \pm 3.2	38.3 \pm 1.5 / 89.6 \pm 0.9 / 64.2 \pm 2.9	51.3 \pm 1.3 / 81.6 \pm 0.3 / 41.2 \pm 0.9

Table 8: Accuracies of each method on coarse-grained INet-A/B test data. OE-based methods here adopt fine-tuning.

\mathcal{D}_{in}	Standard	Rotation [22]	OE [11]	EnergyOE [5]	MixupOE
INet-A	80.8 \pm 0.3	81.1 \pm 0.4	80.3 \pm 0.3	81.2 \pm 0.3	80.2 \pm 0.6
INet-B	81.5 \pm 0.5	81.0 \pm 0.6	80.8 \pm 0.3	81.5 \pm 0.5	80.8 \pm 0.2

I Potential negative societal impacts

In this work, we propose a DNN training algorithm for the problem of OOD detection. Just like many techniques that rely on more sophisticated training procedure to improve OOD detection performance, a net increase in carbon production introduced during the training phase might be considered as a negative impact. We mitigate such problem by adopting the fine-tuning strategy in the primary design and evaluation of our methodology. Meanwhile, with the informed hyperparameter selection, there exists the possibility to reduce excessive training burdens in practice.

OOD samples are pervasive in the “open world” and are a type of threats to machine learning applications, especially those safe-critical ones (e.g., medical screening [15, 16]). As such, by improving detection performance in realistic fine-grained OOD detection settings, MixupOE attempts to induce positive impacts to a broad range of applications that utilize DNN-based systems. Yet, as indicated by the results in Appendix E (e.g., FPR95), it is likely that MixupOE (or any other methods) alone cannot handle real-world OOD detection problems sufficiently well at the current moment. As a result, there still might be certain negative impacts (depending on the applications) to the system when it faces OOD samples that are not successfully identified by MixupOE (or any other methods).